iScience

CellPress
OPEN ACCESS

Review

Wearable triboelectric sensors for biomedical monitoring and human-machine interface

Xianjie Pu,[1] Shanshan An,[1] Qian Tang,[1] Hengyu Guo,[1] and Chenguo Hu[1,*]

SUMMARY

A growing advocacy of healthy and quality life makes wearable electronics spring up. Triboelectric nanogenerator (TENG) has developed as an energy harvesting technology and as an advanced sensor technology in wearable electronics. The triboelectric sensor (TS) is sensitive to the mechanical motion and driven by the motion itself. Therefore, TS is capable of monitoring certain vital signs and kinds of movements of human body. Based on these monitoring, novel human-machine interfaces (HMIs) can be established. In this review, a comprehensive overview of some key progresses in this field over last 5 years are presented. Several main aspects of biomedical monitoring based on TSs are classified: pulse/cardiac/micro-motion, respiration/airflow/vibration, and pressure/tactile/body movement. The major types of HMIs taking these biomedical monitoring as basis are introduced accordingly: eye movement, voice/auditory, gesture/joint movement, and touch/tactile based HMIs. Finally, the current limitations and future trends are put forward for biomedical monitoring and HMIs based on TSs.

INTRODUCTION

With the fast development of micro-nanotechnology, wearable electronics are springing up in the field of health monitoring and smart communication (Bandodkar et al., 2019; Chung et al., 2019; Gao et al., 2016; Pu et al., 2017; Wang et al., 2018c; Zheng et al., 2020). These flexible and light devices greatly improve the quality of life and make life more convenient. A real-time monitoring of the vital signs helps people know their physical conditions better and make timely adjustment for better health and give early warning about a possible disease (Fan et al., 2020; Lin et al., 2018, 2019; Liu et al., 2019a; Zheng et al., 2020). At the same time, this physical information about body conditions and movements may play an important role in the intelligent communication with the surroundings, which is especially meaningful for the assistance for the disabled, industrial production and entertainment (Guo et al., 2016; Osborn et al., 2018; Pu et al., 2017; Si et al., 2020; Wang et al., 2020; Zhu et al., 2020). These demands encourage a development of wearable technology.

Among numerous advanced wearable technologies, triboelectric nanogenerator (TENG) with its significant advantages of self-power, high output, light weight, applicability of design, low cost, stability and robustness etc. has drawn many researchers' attention (Chen et al., 2020; Shi et al., 2019b; Wang, 2020a; Xu et al., 2020). TENG is first invented in 2012 for energy harvesting (Fan et al., 2012; Wang et al., 2012). When two materials have different electronegativity in physical contact, opposite charges generate on the surface of these two materials (Wang and Wang, 2019; Zhou et al., 2020). When they are separated under a mechanical force, the potential created by the charges induces an electron flow through an external circuit (Wang and Wang, 2019; Zhou et al., 2020). Therefore, the applied mechanical force is transformed into electricity. Because TENG can generate electrical signal from a mechanical motion, it can serve as the self-powered sensor for detecting the features of these mechanical movements (Wang, 2013, 2020b; Yang et al., 2013). A triboelectric sensor (TS) can be designed flexibly according to the different application circumstances. There are four basic working modes of TENG, i.e., the contact-separation mode (Zhang et al., 2013, 2017), the linear-sliding mode (Lin et al., 2013; Zhou et al., 2014), the single-electrode mode (Yu et al., 2017; Zhong et al., 2013), and the freestanding triboelectric-layer mode (Guo et al., 2015; Zhang et al., 2015). These four modes have their own unique characteristics and typical application instance, and

[1]Department of Applied Physics, Chongqing Key Laboratory of Soft Condensed Matter Physics and Smart Materials, Chongqing University, Chongqing 400044, P.R. China

*Correspondence: hucg@cqu.edu.cn

https://doi.org/10.1016/j.isci.2020.102027

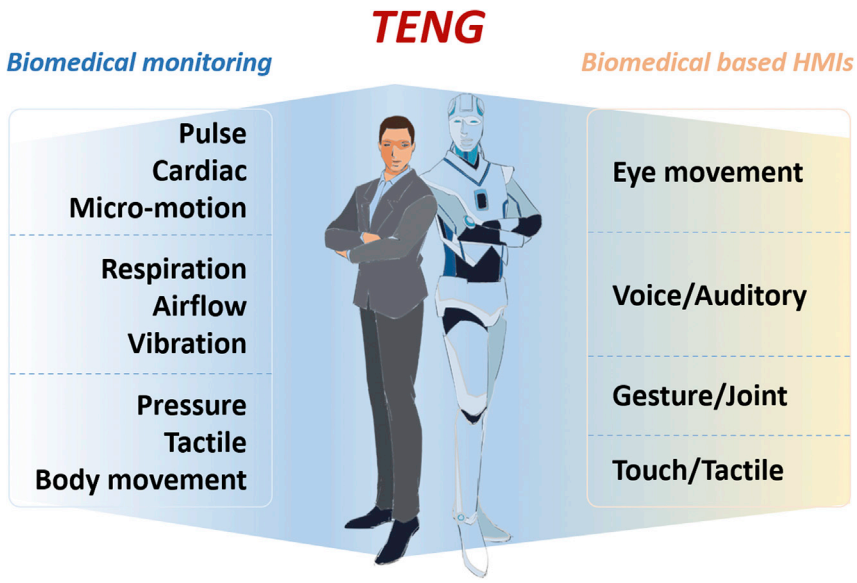

Figure 1. An overview of the wearable triboelectric sensor based biomedical monitoring and HMIs sprung from it

their basic principles will be illustrated following the introduction section. In practice, they are appropriately chosen or used in combination according to specific applications.

This review intends to provide a comprehensive overview of the advances in wearable TSs for the biomedical monitoring and deriving human-machine interfaces (HMIs) in recent 5 years. As shown in Figure 1, the main aspects of biomedical monitoring based on TSs include three-quarters: pulse, cardiac, and micro-motion monitoring; respiration, airflow, and vibration monitoring; and pressure, tactile, and body movement monitoring. The derived HMIs from them are classified accordingly into four parts: eye-movement-based HMIs; voice- and auditory-based HMIs; gesture- or joint-movement-based HMIs; and touch- or tactile-based HMIs. In each part, the application background is briefly introduced, and most articles containing corresponding keywords are cited. Then, several typical examples are illustrated. For a good understanding of each example, the structure and material of the devices, the working principle, and main application performance are sketched accordingly. Further, the problems and potential development trends of wearable TSs for biomedical monitoring and HMIs are addressed for future research.

BASIC WORKING PRINCIPLES OF TRIBOELECTRIC NANOGENERATORS

Contact-separation mode

The vertical contact-separation mode is the most basic mode of TENG, as shown in Figure 2A. When two materials with distinct electron affinity get a physical contact to each other, opposite charges are created on their surfaces. When they are separated by a gap under an external force, the potential is created in the interfacial region and back-deposited electrodes, which drive electrons to flow through the external circuit to keep a balance of the electrostatic field. Once the two materials get contact again, the potential created by the triboelectric charges disappears, thus the induced electrons flow back. On the external load, an alternating output can be detected under the periodic applied force. This mode with simple structure and low wear is easy to design and fabricate, but the requirement of a volume for the varying gap always leads to a packaging difficulty.

Linear-sliding mode

Changing the vertical contact-separation of the two parts into the lateral relative sliding (as shown in Figure 2B), the contact area of the two parts changes along with the sliding, which can also break the electrostatic balance and create a potential to drive the electrons flow through the external circuit. The periodic process is similar to the contact-separation mode. Although, deriving from the basic linear-sliding mode, sliding in planar motions, and cylindrical/disc rotations can also be involved, and multiple grating

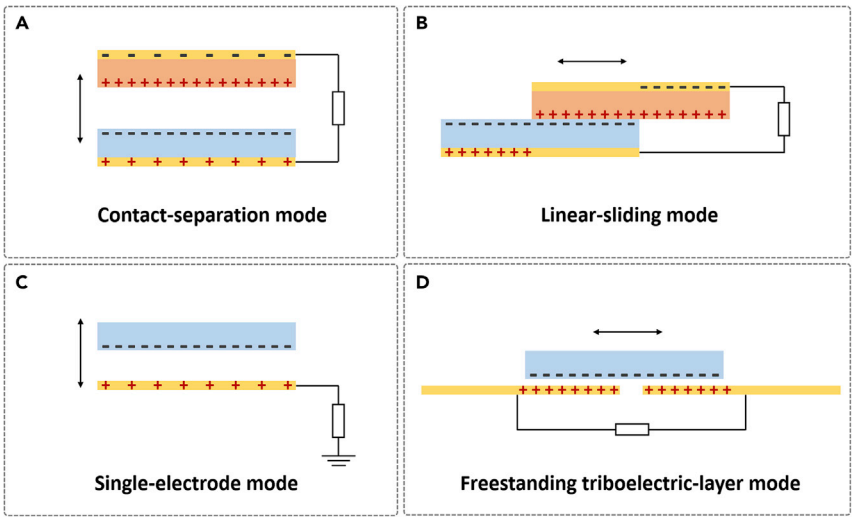

Figure 2. Working mechanism of TENG in four basic modes

Reproduced with permission, from ref (Wang, 2017), Copyright 2017, Elsevier.

(A) The vertical contact-separation mode.

(B) The linear-sliding mode.

(C) The single-electrode mode.

(D) The freestanding triboelectric-layer mode.

structures are developed for certain energy collection purposes or quantitative sensings. However, the frequency friction may reduce the robustness and durability due to wear and tear.

Single-electrode mode

Both the vertical contact-separation mode and linear-sliding mode use a pair of interconnected electrodes with relative displacement, which may limit their applications especially for the mobile object in biomedical sensing and HMIs. Although, the single-electrode mode has only one electrode connected to ground through a load, as shown in Figure 2C. The dielectric part can be freely movable without attaching an electric connection. When the dielectric part periodically approaches to and departs from the stationary electrode via vertical or lateral route, the charges transfer between the electrode and ground. This mode is more flexible but the output performance is lower.

Freestanding triboelectric-layer mode

The freestanding triboelectric-layer mode is a configuration that can keep the pair of electrodes relatively stationary and ground-free. As shown in Figure 2D, the pair of symmetric electrodes are connected to each other with a load. When the dielectric part moves between the two electrodes, an asymmetric charge distribution is created via induction, which causes a charge transfer between the two electrodes through the external load. This mode is always adopted for sliding motions and developed as grating structures based on its features. In practice, these four modes are appropriately chosen and involved in advanced designs for high performances in specific applications.

TRIBOELECTRIC-SENSOR-BASED BIOMEDICAL MONITORING

Pulse/cardiac/micro-motion

Pulse and cardiac wave are typical physiological signals characterizing human conditions (Ma et al., 2018; Ohkuma et al., 2017; Said et al., 2018). The wearable electronics with sensing techniques have important significance in monitoring these body signals for assessment and disease diagnosis (Hui and Kan, 2018; Kim et al., 2012; Park et al., 2018). To date, most wearable sensors are based on force-induced changes in capacitance (Cohen et al., 2012; Lipomi et al., 2011), resistivity (Pang et al., 2012; Wang et al., 2014), piezoelectricity (Persano et al., 2013; Wang and Song, 2006; Wu et al., 2013), and triboelectricity (Chen et al., 2017; Cui et al., 2018; Lai et al., 2017; Liu et al., 2019b; Meng et al., 2019; Yan et al., 2018; Zhao et al., 2019). In fact, the micro-motion caused by the force induced on the skin surface is quite suitable

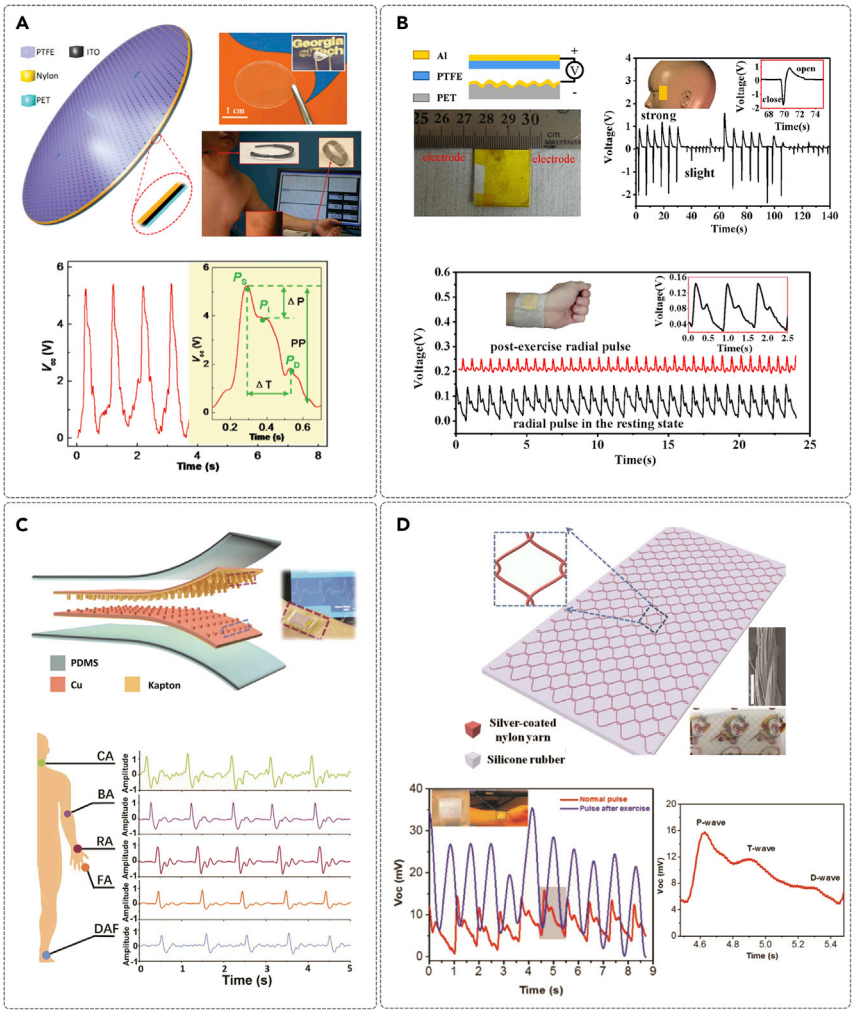

Figure 3. Pulse, cardiac, and micro-motion monitoring based on TSs

(A) Bionic membrane sensor for monitoring the pulse waves. Reproduced with permission, from ref (Yang et al., 2015a), Copyright 2015, WILEY-VCH.

(B) Plat sensor for monitoring muscle motion and pulse waves. Reproduced with permission, from ref (Cai et al., 2016), Copyright 2016, Elsevier.

(C) Elastomer encapsulated sensor for monitoring pulse and the diagnosis system. Reproduced with permission, from ref (Ouyang et al., 2017), Copyright 2017, WILEY-VCH.

(D) Stretchable yarn netting embedded sensor for gauging pressure on skin surface. Reproduced with permission, from ref (Dong et al., 2018), Copyright 2018, WILEY-VCH.

for a self-powered piezoelectric nanogenerator (PENG) or TENG to detect. In contrast with PENG, TENG sensor has relatively higher performance and lower cost. The following are four TENG-based examples: a bionic eardrum sensor for monitoring the pulse waves (Yang et al., 2015a); a plat sensor for monitoring muscle motion and pulse waves (Cai et al., 2016); an elastomer encapsulated sensor for monitoring pulse and the diagnosis system (Ouyang et al., 2017); and a stretchable yarn netting embedded sensor for gauging pressure on skin surface (Dong et al., 2018).

In 2015, Yang et al. introduced a wearable bionic membrane sensor (BMS) for monitoring pulse waves, with a structure inspired by the human eardrum, as shown in Figure 3A (Yang et al., 2015a). The BMS has a multilayer structure in an oval shape with a polyethylene terephthalate (PET) thin film as the substrate. On the PET substrate, a thin layer of nylon film coated with indium tin oxide (ITO) is attached as the electrification layer and the back electrode. On the top, a layer of polytetrafluoroethylene (PTFE) membrane like a human eardrum is tented outward at the level of the tip of an umbo as another electrification layer. Besides, there

are two circular holes punched through the three layers as the communicating vessel to integrate the conical cavity with the ambient air. In the upper-right corner of the figure is the photograph of the as-fabricated transparent BMS. When it is attached onto a subject's carotid artery, chest, and wrist, the detailed information about the arterial physical conditions such as pulse rate, pulse wave velocity (PWV), the augmentation index (AIx), or the reflection index (RI) of carotid artery can be calculated on the parameters of the pulse wave. This BMS can provide a high sensitivity of 51 mV Pa^{-1} with a pressure detection limit to 2.5 Pa as well as a fast response time less than 6 ms. Besides continuous monitoring of the human pulse waves, it can be used as a throat microphone because it holds a wide response frequency ranging from 0.1 kHz to 3.2 kHz.

In 2016, Cai et al. reported a plat sensor for monitoring the muscle motion and pulse waves. This sensor is assembled with two layers: a rough surface PET film deposited with aluminum (R-PET-Al) and a PTFE film deposited with aluminum (PTFE-Al). These two deposited aluminum layers are used as the top and bottom electrodes, respectively, as shown in Figure 3B (Cai et al., 2016). When bonded together, the R-PET-Al film is slightly bent with a distance about 2mm from the PTFE film. Although this structure can be improved, it is the first time to use the TENG to detect the micro muscle motions on the face, which indicates a meaningful development into HMIs and driving fatigue monitoring (Lu et al., 2020; Pu et al., 2017). As demonstrated, when equipped beside the corners of eyes, this sensor can detect and distinguish the strong and slight eyeblink through the amplitude of voltage. When placed over the radial artery of a subject's wrist, the sequentially radial pulse waves in the rest state and right after the exercise can be monitored and identified.

In 2017, Ouyang et al. proposed an elastomer encapsulated self-powered ultrasensitive pulse sensor (SUPS), as shown in Figure 3C (Ouyang et al., 2017). The SUPS consists of two layers spaced to each other. One is a nanostructured Kapton (n-Kapton) thin film as a triboelectric layer, which is deposited with a Cu layer on the back side as one electrode. The other is a nanostructured Cu (n-Cu) film formed through deposition on the previous n-Kapton film, which serves as the other triboelectric layer as well as an electrode. To enhance the structural stability, the entire device is packaged by the polydimethylsiloxane (PDMS) elastomer. Benefiting from the flexibility and super-sensitivity (an output performance of 1.52 V and a signal-to-noise ratio of 45 dB), the SUPS is adaptive to various human body regions and thus can keep a high quality of pulse signals. As shown in Figure 3C, when pasted on the carotid artery, the brachial artery, the radial artery, the finger, and the ankle artery region, the SUPSs detect various amplitudes of pulses with similar features, easy for pulse wave velocity (PWV) calculations. Employing a Bluetooth wireless transmission tech, the pulse wave can be monitored on the intelligent terminals in real time. Based on this, the indicative diagnosis and antidiastole to cardiovascular diseases can be provided through characteristic exponent analysis including heart rate variability (HRV) Poincare plot, time-domain HRV indexes, etc. Therefore, this SUPS shows great value in wearable intelligent mobile diagnosis and cardiovascular disease prevention in the future.

In 2018, Dong et al. focused on the textile-based TENGs to improve the wearability and developed a stretchable yarn netting embedded sensor for sensing pressure on skin surface (Dong et al., 2018). As shown in Figures 3D, a silver-coated nylon yarn with three-ply-twisted configuration is selected as the electrode material, which is interlaced in a "chain-link" fence-shaped network and embedded into the silicone rubber elastomer. This device holds a stretchability of 30% when the basic structure parameters of the yarn network as the height and length are equal to 1.24 mm and the thickness of silicone rubber is 2.8 mm, which covers the strain range of human arm skin. The working principle of this wearable sensor follows a single-electrode mode, and the human skin can be regarded as another triboelectric layer. When attached on the wrist, the real-time arterial pulse waves under normal and exercise conditions can be recorded and distinguished. From the enlarged waveform, the details such as typical percussion wave, tidal wave, and diastolic wave related to the systolic/diastolic blood pressure, the ventricular pressure, and the heart rate can clearly be identified.

Respiration/airflow/vibration

Respiration is another representative signal reflecting the physiological and pathological conditions in health monitoring (Atalay et al., 2015; Massaroni et al., 2018). In addition to being attached to the skin like the pulse sensor, sensing the respiration through the airflow or vibration caused by it is an alternative effective way (Ding et al., 2018; Kim et al., 2019; Sun et al., 2018; Wang et al., 2019a, 2019b; Yi et al., 2015; Zhang et al., 2019a). In this part, these two types of respiration monitoring are reviewed with four examples: first, a chest strap integrated sensor weaved of warp/weft metallic yarns for detecting their intersection

area change in breathing (Zhao et al., 2016); second, an arch structural nanofiber-based permeable sensor integrated inside a mask for detecting the air vibration caused by respiration (Cao et al., 2018b); third, a cellulose fiber based sensor implanted in a mask for breathing detection and $PM_{2.5}$ elimination (He et al., 2018b); fourth, a textile sensor-array-based monitoring system for cardiovascular and respiratory syndrome assessment (Fan et al., 2020).

In 2016, Zhao et al. reported a textile TENG sensor fabricated by weaving of Cu-coated polyethylene terephthalate (Cu-PET) warp yarns and polyimide (PI)-coated Cu-PET (PI-Cu-PET) weft yarns on an industrial loom, as shown in Figure 4A (Zhao et al., 2016). This device eliminates the second-layer structure (Liu et al., 2016). The generation of triboelectric charges depends on the changes of contact area at each yarn crisscross intersection under a mechanic force. The maximum short circuit current density of 15.50 mA m^{-2} can be achieved on it. Integrated into a chest strap, the human respiratory information about rate and depth can be monitored. This flexible device is fabricated with materials widely used in textile industry on miniaturized industrial machines and can withstand standard machine-washing tests. Therefore, it is very promising in wearable healthcare monitoring and other applications.

In 2017, Cao et al. introduced a nanofiber-based triboelectric sensor (SNTS). The SNTS is designed as an arch structure consisting of an electrospun polyvinylidene fluoride (PVDF) nanofiber membrane (NM) and a screen-printed Ag nanoparticles (AgNPs) electrode, as shown in Figure 4B (Cao et al., 2018b). The SNTS follows the working mechanism of single-electrode mode. Due to the different tribo-polarities of PVDF NM and AgNPs, equal amount of positive and negative triboelectric charges will appear on the surface of them when the two tribolayers contact each other. And the AgNPs electrode is connected to the ground through an external load, from which the sensing signal is obtained. Arched inside a mask, the SNTS can monitor the breathing condition. And the SNTS shows a high gas-permeability and stability, and after more than 30 min of breathing, the voltage signal does not decline along with the increase of vapor from human breath.

In 2018, He et al. developed a cellulose-fiber-based TENG simultaneously with $PM_{2.5}$ removal, antibacterial, and breathing monitoring, as shown in Figure 4C (He et al., 2018b). This sensor consists of two dielectric layers applied as tribolayer and both are deposited with an Ag electrode on the backside. The key design of material and structure is introducing 1D biodegradable cellulose nanofibers (CNFs) into the big pores of cellulose microfibers (CMFs) skeleton to form a nanostructured CMFs/CNFs paper. Then, by using the CMFs/CNFs paper as the template, a silver (Ag) nanofibers membrane is fabricated. Finally, a CMFs/CNFs/Ag hierarchical 2D nanostructure is obtained. On the bottom, a fluorinated ethylene propylene (FEP) film as the opposite tribo-material is punched with micro-holes to assist gas flow. Here, CNFs is used to modify the surface for electrification enhancement and to obtain a desirable nanopores-on-micropores 2D structure for particulate matter removal. The Ag nanofibers membrane is simultaneously used as electrode and antibacterial sites. The whole device is mechanically stable and flexible. Implanted in a mask, the device can be triggered by human breathing to induce a voltage signal of 2.22 V at normal status and 3.37 V after a short period of slow running. This wearable device achieves a high efficiency of 98.83% in $PM_{2.5}$ removal, thus it is capable of both improving air quality and healthcare monitoring.

In 2020, Fan et al. reported a triboelectric all-textile sensor array (TATSA)-based healthcare monitoring system (Fan et al., 2020). As shown in Figure 4D, the TATSA is knitted with conductive and nylon yarns in the form of loop interlock units in the course and wale direction. The conductive yarn consists of an inner stainless steel and the wrapped Terylene yarns. There are two kinds of contact surface between the two interlocked yarns, and both will change under an external force due to different stress distribution, thus inducing triboelectric charges transfer. The sensitivity of TATSA is 7.84 mV Pa^{-1}, and the response time is 20 ms. In addition, this textile sensor is flexible and machine washable (>40 washes) and can be integrated into the clothes to dynamically and simultaneously monitor the respiratory and pulse signals. Based on this, a wireless mobile health monitoring system (WMHMS) is developed. As Figure 4D shows, the respiratory and pulse signals of a sleep apnea syndrome (SAS) patient is captured for respiration observation and evaluation, which demonstrates an excellent performance of the TATSA in real time and remote health monitoring.

Pressure/tactile/body movement

Body movement monitoring plays an important role in daily life especially for sports training, medical diagnosis/rehabilitation, and security (Cui et al., 2019; He et al., 2018a; Lin et al., 2018, 2019; Zhang et al., 2019b;

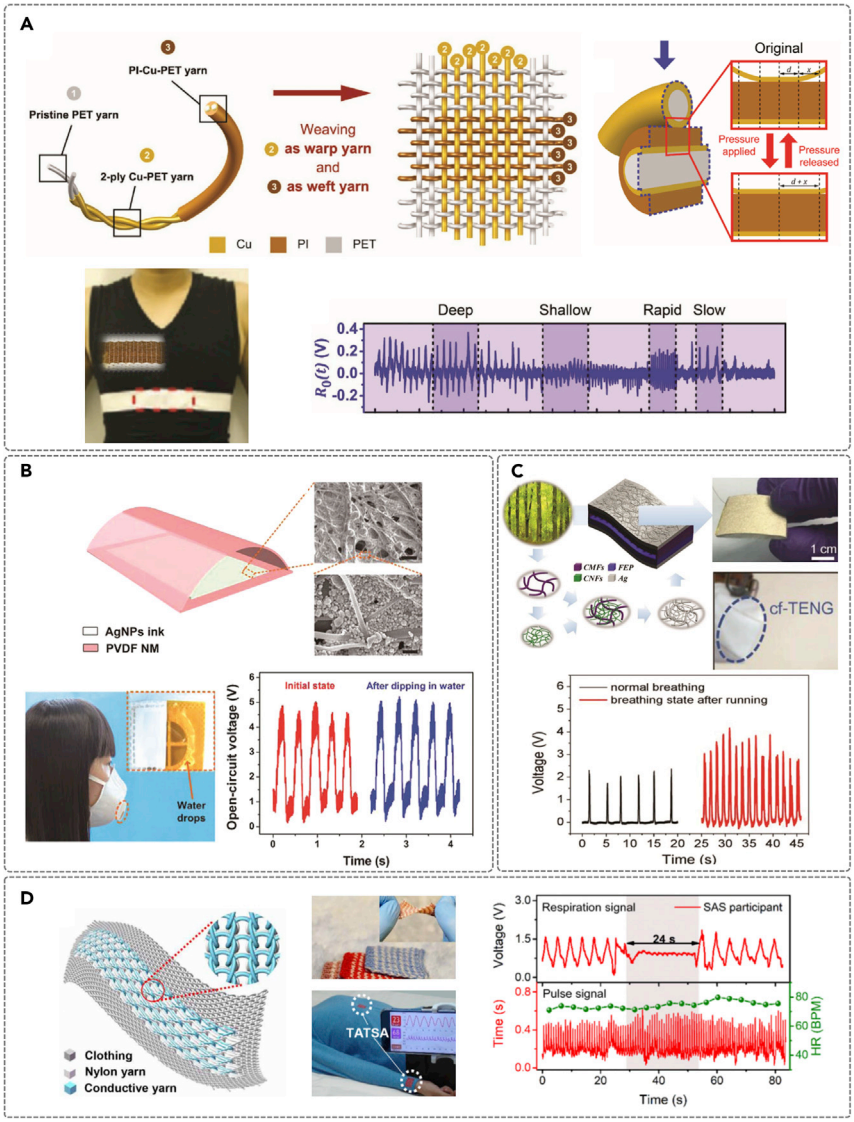

Figure 4. Respiration, airflow, and vibration monitoring based on TSs

(A) Chest strap integrated sensor weaved of warp/weft metallic yarns for detecting their intersection area change in breathing. Reproduced with permission, from ref (Zhao et al., 2016), Copyright 2016, WILEY-VCH.

(B) Arch structural nanofiber-based permeable sensor integrated inside a mask for detecting the respiration caused air vibration. Reproduced with permission, from ref (Cao et al., 2018b), Copyright 2018, Tsinghua University Press and Springer-Verlag GmbH Germany, part of Springer Nature.

(C) Cellulose-fiber-based sensor implanted in a mask for breathing detection and $PM_{2.5}$ elimination. Reproduced with permission, from ref (He et al., 2018b), Copyright 2018, WILEY-VCH.

(D) Textile sensor-array-based monitoring system for cardiovascular and respiratory syndrome assessment. Reproduced with permission, from ref (Fan et al., 2020), Copyright 2020, American Association for the Advancement of Science.

Zou et al., 2019). In these particular applications, the flexibility, stretch ability, and shape-adaptability of sensor are essential for keeping signals stable and device available (Alam et al., 2020; An et al., 2018; Gogurla et al., 2019; Han et al., 2019; Liu et al., 2018; Ma et al., 2020; Sarkar et al., 2019). In this part, five examples based on different fabrications are reviewed: first, a flexible sensor assembled with serpentine-patterned electrodes and wavy-structured Kapton film for detecting the pressing and stretching force in human motions (Yang et al., 2015b); second, an environmentally friendly hydrogel-based tube-shaped TENG for sensing human motions (Xu et al., 2017); third, a shape-adaptive sensor based on a rubber strap covered conductive liquid for biomechanical monitoring (Yi et al., 2016); fourth, a textile-based TENG

sensor for gait monitoring (Jao et al., 2018); fifth, a highly resilient 3D-braided TENG as e-textiles for motion monitoring (Dong et al., 2020b).

In 2015, Yang et al. developed a flexible and stretchable sensor, which was fabricated by assembling a wavy-structured Kapton film and serpentine-patterned electrodes, as shown in Figure 5A (Yang et al., 2015b). The wavy-structured Kapton thin film is sandwiched by two layers of serpentine-patterned copper electrodes, which are deposited on stretchable PDMS substrates. The wavy-structured Kapton thin film serves both as the spacer layer and tribolayer. Due to the orthogonally distributed reversible elastic wavy structure of the Kapton film and the copper electrode, the device can detect both the vertical pressing and horizontal stretching that bring them into contact-separation. This device can withstand a tensile strain of up to 22%. When attached onto the subject's elbow, the bending of the joint leads to the stretching of the device, triggering a voltage signal. When secured on the bicep of an arm, the muscle tensions lead into a pressing force on the device, producing an output voltage too.

In 2016, Xu et al. presented an environmentally friendly hydrogel-based TENG for sensing human motions, as shown in Figure 5B (Xu et al., 2017). The Hydrogel-TENG consists of a flat aluminum (Al) foil layer and a hemispheric shape layer that fabricated by wrapping physical-crosslinking polyvinyl alcohol (PVA) hydrogel in elastic PDMS. The Al foil layer serves as both the tribolayer and electrode. The other electrode is a nickel fabric electrode set in the PVA hydrogel. The whole device is encapsulated by hydrogel. This device is expansible, flexible, and stretchable under an external force, which will cause a change of the contact area between PDMS film and Al layer, leading to a triboelectric charges' flow. Fabricated in a tube-shape, this Hydrogel-TENG can be fixed on the straightened elbow joint. When the joint is bent at different degrees, output voltages are generated accordingly.

In 2016, Yi et al. introduced a shape-adaptive TENG (saTENG) composed of a conductive liquid electrode and a rubber cover, as shown in Figure 5C (Yi et al., 2016). The saTENG can work in the single electrode mode by connecting the inner conductive liquid to the ground through the load. When a positively charged subject approaches the rubber, electrons will flow from the ground to the liquid electrode for keeping an electrostatic balance. If this subject compresses the rubber, the transferred charges increase along with the increased contact area due to deformation. Making a bracelet-like saTENG and wearing it around the upper arm, the bending angle of the forearm can be detected through the output current amplitude affected by the biceps volume increase.

In 2018, Jao et al. developed a chitosan-glycerol-film-based TENG for gait monitoring, as shown in Figure 5D (Jao et al., 2018). This device has a common double-layered structure. One layer is the chitosan-glycerol film, which serves as both triboelectric and conductive materials. The other layer is a PTFE film attached to the metal electrode layer. It is found that chitosan with 20wt% glycerol exhibits largest output voltage. To detect the gait information, the chitosan-glycerol solution is coated onto four points of socks, whereas the layer of PTFE and metal electrode are set on the insole. The four points are set at the toe, inner side of the forefoot, outer side of the forefoot, and heel. According to the force distributions represented by the electric outputs, normal and pigeon-toed walking gait can be distinguished.

In 2020, Dong et al. reported a highly resilient 3D braided TENG as e-textiles for motion monitoring. As shown in Figure 5E (Dong et al., 2020b), The orientation of the braided yarn follows four basic directions, constructing amounts of spatial rhombus-shaped braced frames, which provides enough contact and separation space for them and the inner axial yarn. For these yarns, 8-axial commercial silver-plated nylon yarns form the inner axial yarn, and PDMS is further coated on it to form the braided yarn. Under compression, the inner axial yarn and the braided yarn contact, and the triboelectric charge transfer between the electrodes of these two parts through external circuit occurs. Integrated into the shoe as a rubber encapsulated sole, this textile device can detect the step information such as step number, average velocity, and exercise intensity etc.

BIOMEDICAL MONITORING INTEGRATED HMIS

Eye movement

Mechanosensational HMI as a unique communication channel between humans and external devices plays an important role in helping the disabled and promoting the operation convenience (Barea et al., 2002; Guo et al., 2016; Usakli and Gurkan, 2010). The preliminary works reviewed in part 2.1 (pulse, cardiac and micro-motion monitoring based on TSs) indicate an advantage of TS in mechanosensational HMIs

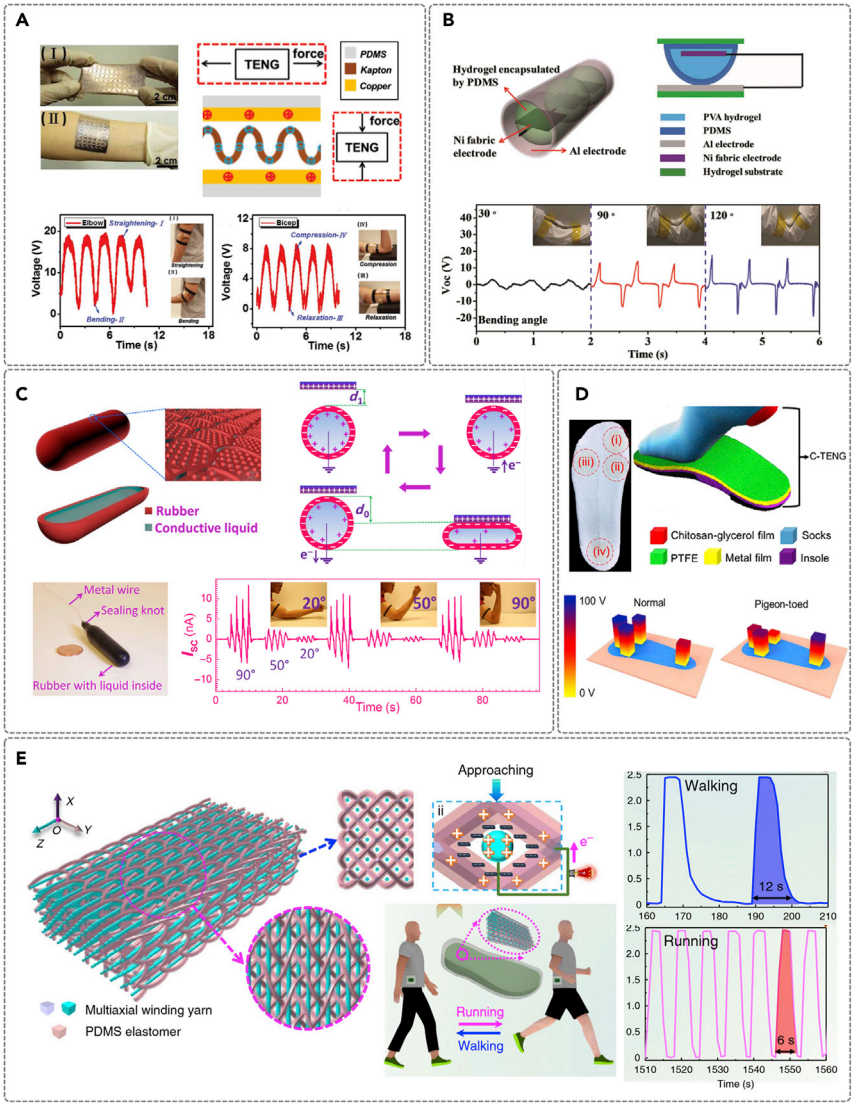

Figure 5. Pressure, tactile, and body movement monitoring based on TSs

(A) Flexible sensor assembled with serpentine-patterned electrodes and wavy-structured Kapton film for detecting the pressing and stretching force in human motions. Reproduced with permission, from ref (Yang et al., 2015b), Copyright 2015, WILEY-VCH.

(B) Environmentally friendly hydrogel-based tube-shaped TENG for sensing human motions. Reproduced with permission, from ref (Xu et al., 2017), Copyright 2017, WILEY-VCH.

(C) Shape-adaptive sensor based on rubber strap covered conductive liquid for biomechanical monitoring. Reproduced with permission, from ref (Yi et al., 2016), Copyright 2016, American Association for the Advancement of Science.

(D) Textile-based TENG sensor for gait monitoring. Reproduced with permission, from ref (Jao et al., 2018), Copyright 2018, Elsevier.

(E) Highly resilient 3D-braided TENG as e-textiles for motion monitoring. Reproduced with permission, from ref (Dong et al., 2020b), Copyright 2020, Springer Nature.

because micro motions even like pulses can be detected by it. The following are two examples of eye-movement-based mechanosensational HMIs: an elastic circular-film-based TS glasses driven by eye-blink for communication (Pu et al., 2017); a near-field transmission-tech-introduced eye movement detection system (Vera Anaya et al., 2020).

In 2017, Pu et al. proposed an aesthetical sensor mounted on a pair of glasses to replace the bioelectrical-based HMI sensors, as shown in Figure 6A (Pu et al., 2017). This sensor follows a multi-film structure based

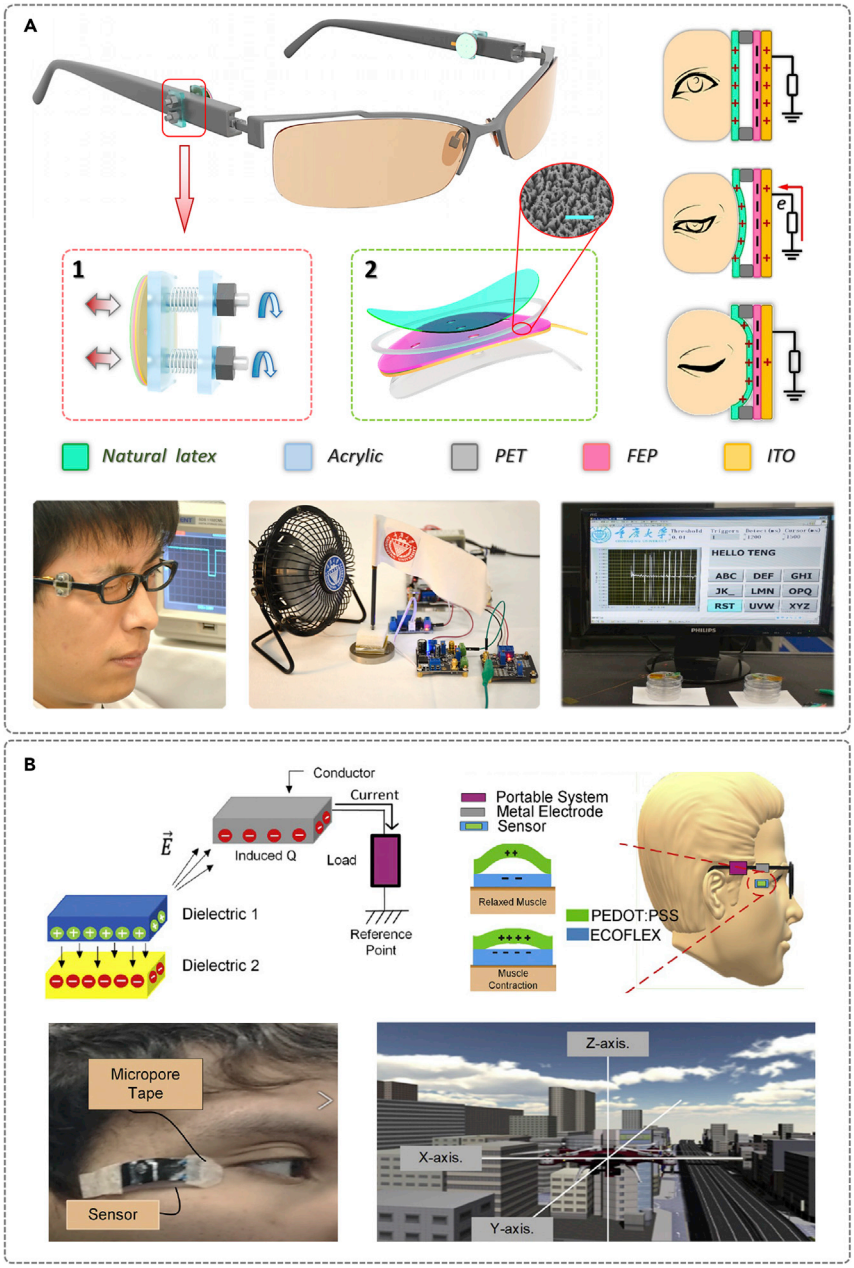

Figure 6. Eye-movement-based HMIs

(A) Elastic circular-film-based TS glasses driven by eye blink for communication. Reproduced with permission, from ref (Pu et al., 2017), Copyright 2017, American Association for the Advancement of Science.

(B) Near-field transmission-tech-introduced eye movement detection system. Reproduced with permission, from ref (Vera Anaya et al., 2020), Copyright 2020, Elsevier.

on a single-electrode mode and could be flexibly mounted on the arm of a pair of glasses through an adjustable fixator. An acrylic thin annulus serves as the spacer between the two tribo-layers to realize a vertical contact/separation driven by the skin motions at the corners of eyes in eye blinking. Through synchronous measurement, it is illustrated that the voltage amplitude of this TS is significantly larger (~750 times) than that of electrooculogram (EOG). Therefore, with a simple signal processing circuit, this TS on a pair of glasses is capable of detecting eye blinking. Setting a threshold, the voluntary and involuntary eye blink can be distinguished and further applied in controlling household appliances and typing on the virtual

keyboard (selecting the corresponding letter by the number of eye blinks). This study brings the TENG to the field of mechanosensational HMIs and may greatly help people achieve a convenient and colorful life.

In 2020, Anaya et al. proposed a non-attached electrode-dielectric approach for monitoring the eye movement based on the near-field transmission tech (Vera Anaya et al., 2020). As shown in Figure 6B, the movement of the oppositely charged elements will create a resultant electric field *E*, which will act on the metal plate in the space similar to a freestanding TENG. The moving elements attached on the lateral skin of the eye are made of a textile layer soaked in poly (3,4-ethylenedioxythiophene): poly (styrene sulfonate) (PEDOT:PSS) solution and an Ecoflex layer, adapted from their work in Ref. (He et al., 2019). The metal plate is fixed on one arm of the spectacles close to the friction layers, beside which a box packaged with the conditioning circuit, microcontroller, and Bluetooth is also fixed. This sensing system is applied in the cursor and virtual drone control, by blinking different number of times to select the directions.

Voice/auditory

Voice is the most natural form of communication. Li et al. have reported a ferroelectret nanogenerator-based dual-functional acoustic device (as loudspeaker or microphone) (Li et al., 2017). Whereas, a smart microphone itself can play a dual-functional role in HMIs. As Yang et al. expected from the social robotics, the smart machine (e.g. a humanoid robot) needs a sensitive electronic ear, like a human being needs the normal hearing (Yang et al., 2018). A good hearing aid is to amplify the specific impaired frequency regions to audible levels (Meyer and Hickson, 2012; Popelka et al., 1998). Therefore, to enhance voice communication in HMIs, a sensitive acoustic sensor with a simple structure, broader frequency response, and frequency selectivity is highly desired (Fan et al., 2015). In this part, two examples of TENG-based acoustic sensor are reviewed: a triboelectric-based artificial basilar membrane (TEABM) to mimic cochlear tonotopy (Jang et al., 2016); a circular-type single-channel triboelectric auditory sensor (TAS) for both robotics and human beings (Guo et al., 2018).

In 2016, Jang et al. reported a basilar-membrane-inspired triboelectric acoustic sensor for acoustic-to-electric conversion (Jang et al., 2016). As shown in Figure 7A, the conceptual schematic of the organ of Corti illustrates the movement of basilar membrane, which induces an acoustic-to-electric transduction. Inspired by it, the triboelectrification between materials with different electronegativity can be used to implement this transduction. In this device, there are eight fixed beams with different lengths to respond at different resonance frequencies. Each beam is stacked with an Al foil (bottom layer) and a Kapton film sputtered with Au as electrode (top layer). The Al layer is connected to the Au layer through an external circuit. When the beam vibrates at the resonance frequency of the acoustic stimulus, triboelectricity is generated by vertical contact separation of the two layers. The bottom left subfigure shows the resonance frequency (i.e., the peak) sequentially shifts to a lower frequency as the channel number increases (i.e., with increasing beam length). With frequency selectivity from 294.8 to 2311 Hz, the sensitivity is measured in the range of 1.74–13.1 mV Pa^{-1}. As the author described, the minimum sound pressure level (SPL) to drive this TEABM is around 70 dB_{SPL}. In the range of 70–85 dB_{SPL}, on a deafened guinea pig model, the clear electrically evoked auditory brainstem response (eABR) is recorded, which is elicited by the stimulating pulses converted from TEABM's output.

In 2018, Guo et al. proposed a circular-type single-channel TAS for building an electronic hearing device for both robotics and humans (Guo et al., 2018). As shown in Figure 7B, the inner free Kapton film sputtered with Au vibrates under air flow, inducing the triboelectricity due to the contact-separation with the upper FEP film. This tiny, thin, and even transparent device shows ultra-high sensitivity up to 110 mV/dB. Further, based on the design of annular or sectorial inner boundary architecture, the resonant frequency band is tunable and the response band can be extended to the range of 100–5000 Hz, which almost covers the whole frequency range of human voice. Therefore, the TAS can be fabricated as the robotics' electronic ear for communicating with humans. For helping the humans with hearing loss, this TAS can be set at the front end of the hearing aid system to respond to the lost frequency bands only, which can be realized by adjusting the proportion of inner-bounded partitions. Then, the response signal is amplified in a single channel to the normal level, without affecting the original normal frequency bands because there are only the response and amplification of the lost frequency bands in the process. This prototype different from ordinary signal processing is demonstrated on a hearing-impaired model established by weakening the sound to −30 dB in the 207 to 837 Hz and the 1594 to 2090 Hz frequency bands. At last, the impaired frequency bands are rehabilitated by the TAS-based processing system.

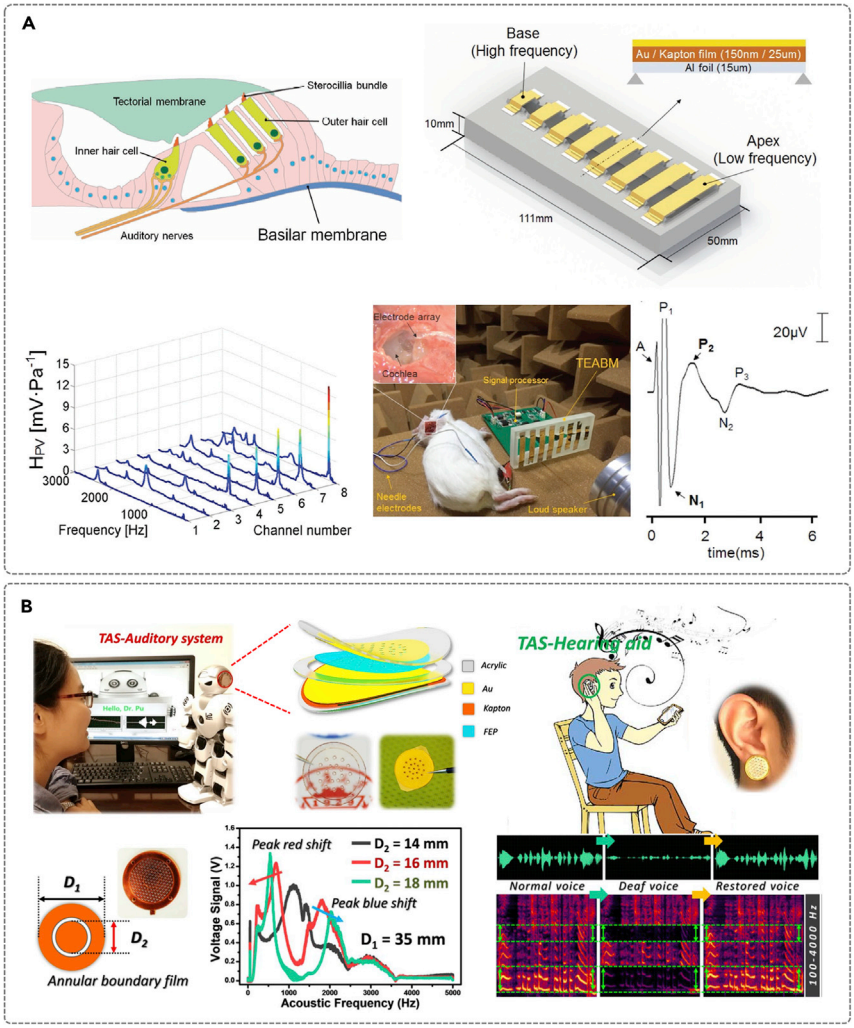

Figure 7. Voice- and auditory-based HMIs

(A) Triboelectric-based artificial basilar membrane (TEABM) to mimic cochlear tonotopy. Reproduced with permission, from ref (Jang et al., 2016), Copyright 2016, WILEY-VCH.

(B) Circular-type single-channel triboelectric auditory sensor (TAS) for both robotics and human beings. Reproduced with permission, from ref (Guo et al., 2018), Copyright 2018, American Association for the Advancement of Science.

Gesture/joint

In manufacturing industry, medical care/rehabilitation, and disaster relief etc., gesture interaction with machine is an intuitive approach to reduce difficulties and costs in learning (Chen et al., 2019; Chiu et al., 2019; He et al., 2019; Yang et al., 2018). To realize a precise control of the machine, quantification of the motion information is requisite (Dong et al., 2020a; Pu et al., 2018; Wang et al., 2020; Zhu et al., 2020). In this part, four kinds of wearable TENG-based gesture/joint motion sensors and interaction systems are reviewed: first, a stretchable kinesio-tape-based TS for gesture monitoring via amplitude quantification (Wang et al., 2018b); second, a grating structured sensor quantifying joint rotation via counting the induced positive/negative pulses and the transient control of robot hand (Pu et al., 2018); third, a rotating grating structured angle sensor for robotic arms via counting pulses and detecting phase difference (Wang et al., 2020); and fourth, a nanophotonic readout tech integrated sensor system for intermediate state sensing (Dong et al., 2020a).

In 2018, Wang et al. reported a stretchable kinesio-tape-based motion sensor relying on the lateral sliding TENG mode, as shown in Figure 8A (Wang et al., 2018b). This device is composed of two tribolayers (PET and Kapton films) with back electrode on each and two kinesio tapes as substrates to fasten the opposite ends of

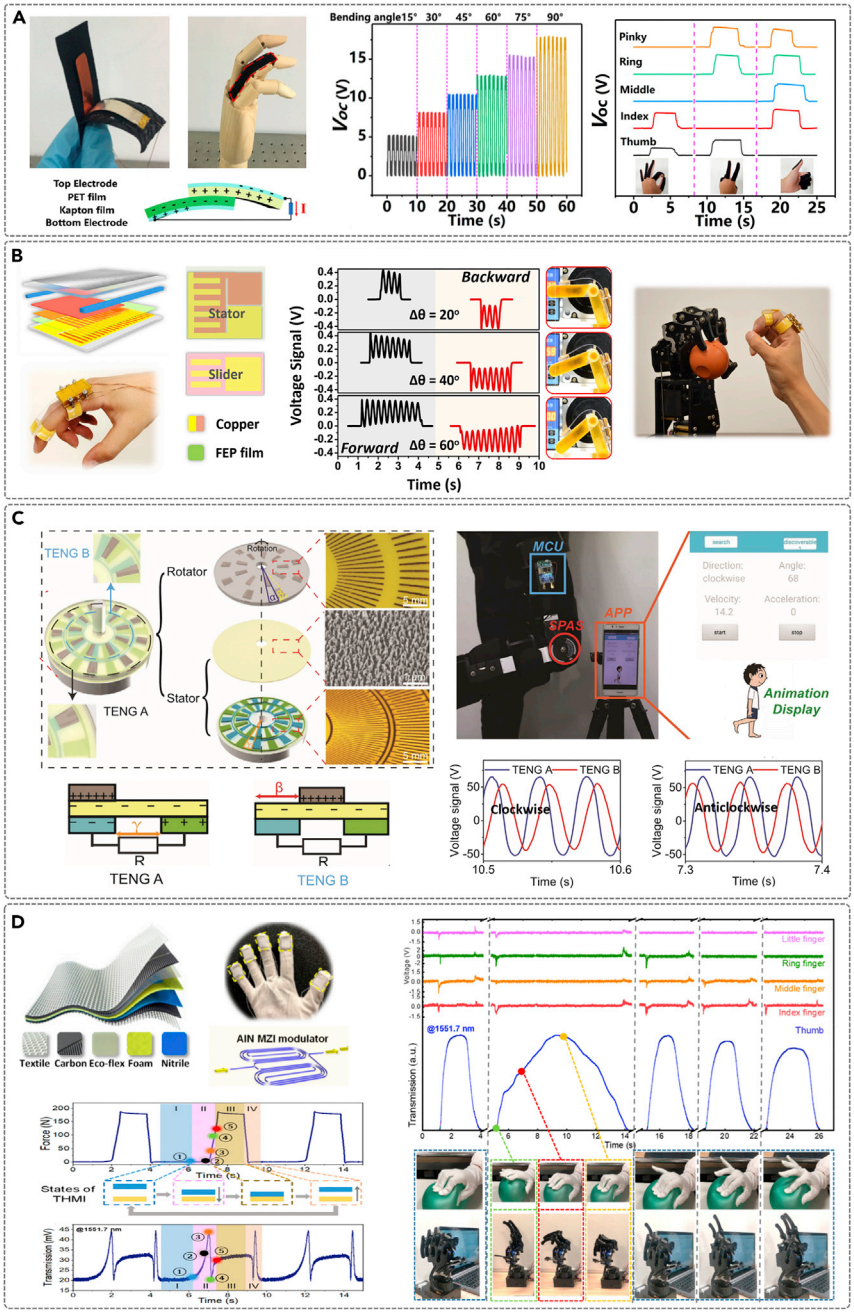

Figure 8. Gesture or joint-movement-based HMIs

(A) Stretchable kinesio-tape-based TS for gesture monitoring via amplitude quantification. Reproduced with permission, from ref (Wang et al., 2018b), Copyright 2018, MDPI.

(B) Grating structured sensor quantifying joint rotation via counting the induced positive/negative pulses and the transient control of robot hand. Reproduced with permission, from ref (Pu et al., 2018), Copyright 2018, Elsevier.

(C) Rotating grating-structured angle sensor for robotic arms via counting pulses and detecting phase difference, the scale bars are 5 mm, 1 μm. Reproduced with permission, from ref (Wang et al., 2020), Copyright 2020, WILEY-VCH.

(D) Nanophotonic readout tech-integrated sensor system for intermediate states sensing. Reproduced with permission, from ref (Dong et al., 2020a), Copyright 2020, American Chemical Society.

them, respectively. When attached onto the joint of a finger, the bending strain will stretch the tapes crookedly and initiate the inner ends fixed tribolayers to slide relatively, inducing a potential difference between the two back electrodes to drive a charge flow through the external circuit. Because the separate surface area is linearly correlated to the bending angles, the amplitude of output voltage can directly reflect the bending state. This quantification based on amplitude has been adopted in many researches (Alam et al., 2020; Han et al., 2019; Liu et al., 2020; Yu et al., 2019). As a demonstration, five such kind of sensors are attached on to the fingers to monitor the motion of each finger and different gestures.

In 2018, Pu et al. designed a grating structured joint motion triboelectric quantification sensor (jmTQS) to detect the flexion/extension degree and speed of the finger by counting the positive/negative pulses generated in unit time, as shown in Figure 8B (Pu et al., 2018). Through a hinge model, it is verified that the rotation angle is linear to the tensile displacement at the finger joint. This kind of tensile displacement can be detected by the sliding freestanding mode. As the figure shows, the slider and the stator have the corresponding patterns of electrode grids to simultaneously induce wide and narrow pulses in sliding, which represent the direction and degree respectively. Therefore, through counting the narrow pulses of the output coupling signal in unit time, the rotation angle and speed can be judged; through the positive or negative of coupling signal, the rotation direction can also be judged. At last, the demonstration shows jmTQS can directly quantify the joint flexion, extension, and speed and can be further applied in the synchronous control of a robotic hand with intermediate states.

In 2020, Wang et al. reported a rotating grating-structured self-powered angle sensor (SPAS) for applying in robotic arms and recording the flexion and extension of joints, as shown in Figure 8C (Wang et al., 2020). The SPAS is based on a sliding freestanding mode, consisting of a rotator and a stator coaxially assembled. The rotator part includes two groups of radial freestanding electrodes, with the same central angle of α and a central angle phase difference of β between them. The outer circle group belongs to TENG A (inducing the sensing signal), whereas the inner circle group belongs to TENG B (inducing the reference signal). The stator part is composed of a tribolayer film and two groups of radial interdigital electrodes corresponding to the two groups of freestanding electrodes in the rotator. The central angle of the two groups of electrodes in the stator is the same, which causes a difference in the overlaps of rotator-stator electrodes between TENG A and B. Taking clockwise-rotation as an example, owing to the difference in the overlaps, the freestanding electrode in the inner circle TENG B is ahead of that in the outer circle TENG A, forming a phase difference between the reference and sensing signals and vice versa. Therefore, the rotation direction can be judged by the phase difference. To judge the overall rotation angle and angular velocity, counting the number of pulses and dividing it with the spent time produces the results, similar to the aforementioned work. In addition, the author proposed another scheme to improve the angular resolution via establishing the correspondence between rotation angles and voltage signals in a unit period based on linearization of the voltage ramp. As a demonstration, the SPAS is assembled in a medical brace to record joint's flexion/extension movement, indicating its application in personalized recuperation and rehabilitation robots.

In 2020, Dong et al. proposed a nanophotonic readout tech integrated sensor system for intermediate states sensing (Dong et al., 2020a). Conventionally, TENG tech generates pulse signals on the basis of transient charge flow and uses electrical readout, which may lead to unstable and lossy transmission of interaction information. As shown in Figure 8D, the common textile TS is composed of a positive nitrile layer with carbon cloth, a thin foam spacer, and a negative Ecoflex-coated carbon cloth, encapsulated in two pieces of nonconductive textiles. Specifically, this sensor's output is applied to a nanophotonic aluminum nitride (AlN) Mach–Zehnder interferometer (MZI) modulator, which is composed of an AlN MZI sandwiched in a micro parallel-plate capacitor. When the TENG sensor works in open-circuit condition, the current flow can be negligible, thus the electrical state induced by different stimuli can be maintained. Although, according to the electro-optic Pockels effect, the optical transfer in the AlN MZI can be changed by the open-circuit voltage generated. Due to high data transmission rate of the nanophotonic readout and the open-circuit condition enabled by it, various linear force sensitivity can be achieved independent of the force speed. At last, a robotic hand control is distinctively demonstrated by detecting the grasp force applied on a balloon to reflect the gesture intermediate process.

Touch/tactile

The overwhelming majority of HMIs relies on tactile interactions (Cao et al., 2018a; Guo et al., 2020; Huang et al., 2020; Kang et al., 2019; Meng et al., 2018; Wu et al., 2018b, 2020; Xue et al., 2016; Yuan et al., 2017).

From the traditional keyboards (Ahmed et al., 2017; Chen et al., 2015; Jeon et al., 2018; Wang et al., 2018a; Wu et al., 2018a; Yang et al., 2013) and touch pads (Chen et al., 2018; Dong et al., 2018; Shi et al., 2019a) to the rising electronic skin (Chang et al., 2020; Lai et al., 2016, 2019; Wu et al., 2017), the tactile sensors are developed to be more flexible, sensitive, efficient, and multi-functional, even with human-like intelligence. In this part, six examples of TENG-based tactile sensors are reviewed: a high-resolution pressure-sensitive TS matrix for tactile mapping (Wang et al., 2016); an elastic metal-free tactile sensor for detecting both normal and tangential forces (Ren et al., 2018); a transparent and attachable ionic hydrogel-based pressure sensor for coded communication (Lee et al., 2018); a flexible touch pad with subdivided units for tactile XY positioning (Pu et al., 2020); a user-interactive electronic skin for touch track mapping based on the triboelectric-optical model (Zhao et al., 2020); and a triboelectric tactile sensor producing various amplitudes of signals based on the history of pressure stimulations for mimicking neuromorphic functions of synaptic potentiation and memory (Wu et al., 2020).

In 2016, Wang et al. reported a high-resolution pressure-sensitive triboelectric sensor matrix (TESM) for tactile mapping, as shown in Figure 9A (Wang et al., 2016). The TESM follows a single-electrode design of TENG, and each sensing unit serves as one channel. To reduce the overwhelming wiring difficulty, the electrode is deposited on both sides of the flexible PET substrate interconnected with each other via through-holes. The regular electrode arrays on the top side serve as the charge sensing elements, whereas the electrodes on the bottom side serve as the wiring elements and are connected to the external measuring equipment. Then, the bottom side is encapsulated by another thin film of PET with ethylene–vinyl acetate copolymer (EVA). On the top side, a PDMS film is spin-coated as a tribolayer relative to the contact object. In this configuration, a 16 × 16 pixelated TESM with a resolution of 5 dpi is fabricated, which can map both single-point and multi-points touch via multichannel acquisition. In addition, this configuration has been improved to be a cross-type to reduce the number of addressing lines from m × n to m + n, which benefits the real-time tactile mapping but sacrifices the multi-points mapping.

In 2018, Ren et al. demonstrated a fully elastic tactile sensor for detecting both normal and tangential forces, which is essential for mimicking human tactile pressure but always overlooked by most of the previous studies (Ren et al., 2018). As shown in Figure 9B, with the single-electrode mode, this TENG consists of an elastic PDMS film as the tribolayer and four stretchable PDMS-carbon black mixture (PDMS-CB) electrodes arrayed on an elastic PDMS substrate. Specifically, tiny burr arrays are printed on the electrification surfaces of PDMS tribolayer and PDMS-CB electrodes layer, respectively. Under normal force, the elastic deformation of PDMS film and the compression deformation of tiny burr arrays on the four electrode regions will uniformly lead to a potential change, thus driving a charge flow through the external circuit. Under the tangential force, the shear deformation of tiny burr arrays and elastic deformation of the PDMS layer in 2D region will lead to nonuniform changes of the overlapping tiny burr areas on the four electrodes, inducing different potential changes on these four electrodes. Take the tangential force applied along 45° direction as an example, the output voltages from E1~E3 electrodes increase, whereas the output voltage from E4 electrode decreases.

In 2018, Lee et al. reported a self-cleanable, transparent, and attachable ionic hydrogel-based pressure sensor for coded communication, as shown in Figure 9C (Lee et al., 2018). Firstly, the PDMS and hydrogel (as an ionic conductor) is chemically anchored to each other, overcoming the weak physical bonding due to the difference in affinities to water and Young's modulus. Then, using an (heptadecafluoro-1,1,2,2-tetrahydrodecyl) trichlorosilane (HDFS) chemical surface treatment, an anti-contaminated contact surface is obtained along with maximizing contact electrification and transparency. This stable, highly stretchable, transparent and soft sensor can be attached onto five fingers with thimble type, to send words by coding each finger's tactile signal to interpret to an alphabet.

In 2020, Pu et al. presented a flexible 3D triboelectric touch pad (3D-TTP) with subdivided units for tactile XY positioning (Pu et al., 2020). As shown in Figure 9D, this 3D-TTP consists of two parts: the top three layers for XY positioning and the bottom three layers for pressure sensing. For tactile mapping, the matrix scheme can greatly reduce the number of channels and achieve a high-resolution wiring layout. However, new problems about crosstalk and target sensing resolution arise. To address these problems, an XY complementary subdivision pattern (XYCSP) of two layers of orthogonal electrodes is proposed, as shown in the figure. This XYCSP configuration can suppress the crosstalk through reducing the overlap area of these two layers of orthogonal electrodes as well as make object positioning robust in object size and contact

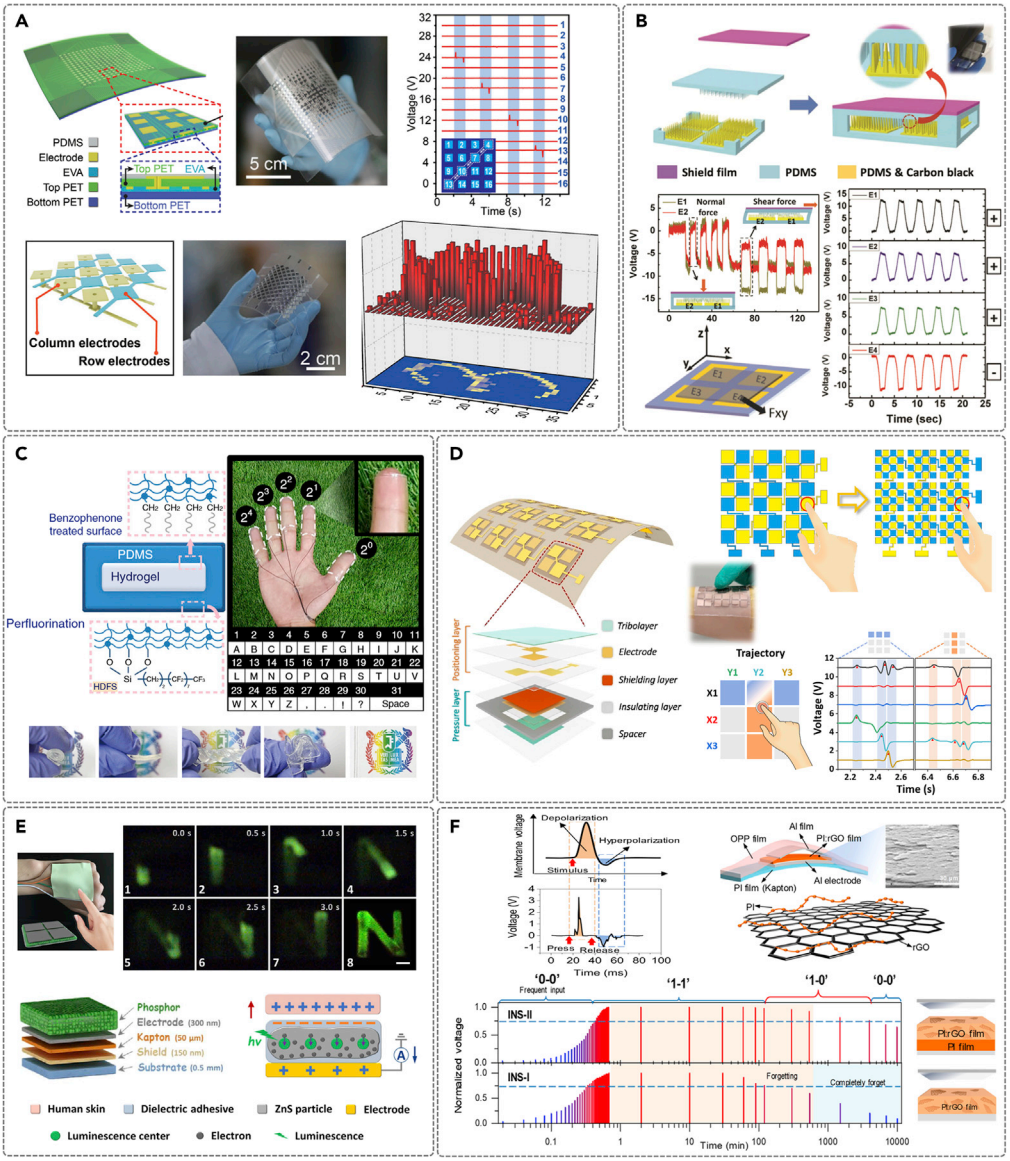

Figure 9. Touch- or tactile-based HMIs

(A) High-resolution pressure-sensitive TS matrix for tactile mapping. Reproduced with permission, from ref (Wang et al., 2016), Copyright 2016, WILEY-VCH.

(B) Elastic metal-free tactile sensor for detecting both normal and tangential forces. Reproduced with permission, from ref (Ren et al., 2018), Copyright 2018, WILEY-VCH.

(C) Transparent and attachable ionic hydrogel-based pressure sensor for coded communication. Reproduced with permission, from ref (Lee et al., 2018), Copyright 2018, Springer Nature.

(D) Flexible touch pad with subdivided units for tactile XY positioning. Reproduced with permission, from ref (Pu et al., 2020), Copyright 2020, Elsevier.

(E) User-interactive electronic skin for touch track mapping based on the triboelectric-optical model. Reproduced with permission, from ref (Zhao et al., 2020), Copyright 2020, American Association for the Advancement of Science.

(F) Triboelectric tactile sensor producing various amplitudes of signals based on the history of pressure stimulations for mimicking neuromorphic functions of synaptic potentiation and memory. Reproduced with permission, from ref (Wu et al., 2020), Copyright 2020, American Chemical Society.

point. As a proof, the tactile signal mapping the finger trace of "T" on a 3 × 3 pad is demonstrated without an additional shielding layer between the two layers of orthogonal electrodes. In addition, with the bottom-attached pressure sensing layer, an anti-peek password-based authentication is demonstrated.

In 2020, Zhao et al. introduced a self-powered user-interactive electronic skin (SUE-skin) for converting touch stimuli into electrical signals and visible lights simultaneously, as shown in Figure 9E (Zhao et al., 2020). The SUE-skin consists of a phosphor layer, an Al electrode, a Kapton layer, an Al shield layer, and a PDMS substrate. The phosphor layer here is fabricated with the synthesis of ZnS (ZnS: Cu, Al) phosphor particles, which has higher luminous efficiency than traditional ZnS: Cu due to the co-activation of doped Al. A triboelectric-optical model is proposed to explain the ability of the SUE-skin to realize touch visualization and mapping at a low-pressure threshold. When the human-skin gradually separates from the initial contact state with SUE-skin, the negatively charged surface of the dielectric adhesive will induce a current flow to the electrode through the external circuit, leading to an inner varying electric field to drive the electrons produced by the impact ionization toward the bottom ZnS phosphor particle, probably exciting the luminescence centers and causing electroluminescence. When the human-skin gradually approaches the SUE-skin again, the electrons inside the ZnS will move in reverse under the varying electric field, exciting the luminescence centers and causing electroluminescence again. As a demonstration, four channels of SUE-skin are fabricated to control the consumer electronics, showing an intuitive touch lighting and track mapping.

In 2020, Wu et al. proposed a novel triboelectric tactile sensor to mimicking neuromorphic functions of synaptic potentiation and memory, as shown in Figure 9F (Wu et al., 2020). The device follows a common single-electrode mode and adopts an arch-shaped structure design to achieve a longer duration time of separation (release) process than contact (press) process, which leads to a higher positive-polarity voltage than the negative one just as the biological action potentials generated by mechanoreceptors. Furthermore, as a key component, the reduced graphene oxides (rGOs) is embedded in the negative friction layer (PI film) to act as electron-body traps to elongate the time interval to reach a saturation state. In this model, the output voltage shows a temporary increase, as well as a spontaneous decay over time. Therefore, under certain times of pressure stimuli, the output voltages increase to exceed a threshold, just like the accumulated biological excitatory postsynaptic potential (EPSP) making the post synaptic neuron to fire an action potential ("0" to "1"). The stacked structure in the friction layer is used to mediate the retention time of the information to realize a short-term memory (STM, of INS-I) and a long-term memory (LTM, of INS-II). This work emulated a combined mechanoreceptor and neuromorphic system, based on which, the two-dimensional information of the current and previous stimulation can be recorded.

CONCLUSION AND PROSPECTS

In this review, we investigate the recent developments in wearable TSs for biomedical monitoring and the HMIs that take the biomedical monitoring as basis. For biomedical monitoring, wearable TSs are mainly used to monitor pulse and related cardiac state, respiration, and some physical movements that cause stress or stretch. For HMIs, wearable TSs are mainly applied in the control stage by detecting eye-movement, voice, gesture, and touch signals, as well as a few applications in the feedback phase as hearing aids, rehabilitation robots, and electronic skin. Among these researches, some devices are designed as general devices for various scenes, whereas more designs focus on specific scenarios to bring forward optimal designs, which jointly promote the development of this research field. For future research, several suggestions are proposed:

1 From the wearable point of view, the materials used in biomedical monitoring and HMIs are expected to be flexible, light, stretchable, washable, aesthetic, skin friendly, and even environmentally friendly. Therefore, researchers will gradually make use of textile, rubber, hydrogel, shape memory polymers, and other novel functional materials to fabricate TENG sensor with well-designed structures.

2 In the aspect of sensing strategy, quantification is proposed to replace the conventional two-stage judgment (i.e., "0" and "1") on a transient pulse without any intermediate state, especially for the control stage. In addition, the composite mechanism of the intermediate state in a human-like intelligent sensor (e.g., electronic skin) still needs to be explored.

3 In terms of signal processing, the essential signal processing and wireless transmission device should be highly integrated, with the features of small size, anti-interference, and low power consumption. TENG's power generating nature and the corresponding power management can be integrated for a fully self-powered mobile system. Besides, advanced algorithms based on machine learning and big data etc. are also essential for the robust biomedical monitoring and HMIs in daily applications.

4 From the perspective of technical integration, multiparameter system can be founded with advanced packaging and optimized modularization, and more other technologies like near-field transmission, nanophotonic readout, electroluminescence, and several wireless sensing technologies etc., can be appropriately introduced to promote the development of wearable biomedical monitoring and HMIs.

ACKNOWLEDGMENTS

This work was supported by National Natural Science Foundation of China (NSFC) (51902035, 52073037 and 51572040), Natural Science Foundation of Chongqing (cstc2020jcyj-msxmX0807), the Fundamental Research Funds for the Central Universities (2020CDJ-LHSLNSS-001, 2019CDXZWL001 and 2020CDCGJ005), and Chongqing Graduate Tutor Team Construction Project (ydstd1832).

AUTHOR CONTRIBUTIONS

X.P. wrote the manuscript and prepared the figures. S.A. collected the literature. Q.T. and H.G. cooperated in the related research. C.H. discussed and revised the manuscript.

REFERENCES

Ahmed, A., Zhang, S.L., Hassan, I., Saadatnia, Z., Zi, Y., Zu, J., and Wang, Z.L. (2017). A washable, stretchable, and self-powered human-machine interfacing Triboelectric nanogenerator for wireless communications and soft robotics pressure sensor arrays. Extreme Mech. Lett. *13*, 25–35.

Alam, M.M., Lee, S., Kim, M., Han, K.S., Cao, V.A., and Nah, J. (2020). Ultra-flexible nanofiber-based multifunctional motion sensor. Nano Energy *72*, 104672.

An, S., Sankaran, A., and Yarin, A.L. (2018). Natural biopolymer-based triboelectric nanogenerators via fast, facile, scalable solution blowing. ACS Appl. Mater. Inter. *10*, 37749–37759.

Atalay, O., Kennon, W.R., and Demirok, E. (2015). Weft-knitted strain sensor for monitoring respiratory rate and its electro-mechanical modeling. IEEE Sens. J. *15*, 110–122.

Bandodkar, A.J., Gutruf, P., Choi, J., Lee, K., Sekine, Y., Reeder, J.T., Jeang, W.J., Aranyosi, A.J., Lee, S.P., Model, J.B., et al. (2019). Battery-free, skin-interfaced microfluidic/electronic systems for simultaneous electrochemical, colorimetric, and volumetric analysis of sweat. Sci. Adv. *5*, eaav3294.

Barea, R., Boquete, L., Mazo, M., and Lopez, E. (2002). System for assisted mobility using eye movements based on electrooculography. IEEE Trans. Neural Syst. Rehabil. Eng. *10*, 209–218.

Cai, F., Yi, C., Liu, S., Wang, Y., Liu, L., Liu, X., Xu, X., and Wang, L. (2016). Ultrasensitive, passive and wearable sensors for monitoring human muscle motion and physiological signals. Biosens. Bioelectron. *77*, 907–913.

Cao, R., Pu, X.J., Du, X.Y., Yang, W., Wang, J.N., Guo, H.Y., Zhao, S.Y., Yuan, Z.Q., Zhang, C., Li, C.J., et al. (2018a). Screen-printed washable electronic textiles as self-powered touch/gesture tribo-sensors for intelligent human-machine interaction. ACS Nano *12*, 5190–5196.

Cao, R., Wang, J., Zhao, S., Yang, W., Yuan, Z., Yin, Y., Du, X., Li, N.-W., Zhang, X., Li, X., et al. (2018b). Self-powered nanofiber-based screen-print triboelectric sensors for respiratory monitoring. Nano Res. *11*, 3771–3779.

Chang, Q., He, Y., Liu, Y., Zhong, W., Wang, Q., Lu, F., and Xing, M. (2020). Protein gel phase transition: toward superiorly transparent and hysteresis-free wearable electronics. Adv. Funct. Mater. *30*, 1910080.

Chen, J., Zhu, G., Yang, J., Jing, Q.S., Bai, P., Yang, W.Q., Qi, X.W., Su, Y.J., and Wang, Z.L. (2015). Personalized keystroke dynamics for self-powered human-machine interfacing. ACS Nano *9*, 105–116.

Chen, T., Shi, Q., Zhu, M., He, T., Sun, L., Yang, L., and Lee, C. (2018). Triboelectric self-powered wearable flexible patch as 3D motion control interface for robotic manipulator. ACS Nano *12*, 11561–11571.

Chen, T., Shi, Q.F., Zhu, M.L., He, T.Y.Y., Yang, Z., Liu, H.C., Sun, L.N., Yangt, L., and Lee, C. (2019). Intuitive-augmented human-machine multidimensional nano-manipulation terminal using triboelectric stretchable strip sensors based on minimalist design. Nano Energy *60*, 440–448.

Chen, X., Song, Y., Su, Z., Chen, H., Cheng, X., Zhang, J., Han, M., and Zhang, H. (2017). Flexible fiber-based hybrid nanogenerator for biomechanical energy harvesting and physiological monitoring. Nano Energy *38*, 43–50.

Chen, X.P., Xie, X.K., Liu, Y.N., Zhao, C., Wen, M., and Wen, Z. (2020). Advances in healthcare electronics enabled by triboelectric nanogenerators. Adv. Funct. Mater. *30*, 2004673.

Chiu, C.M., Chen, S.W., Pao, Y.P., Huang, M.Z., Chan, S.W., and Lin, Z.H. (2019). A smart glove with integrated triboelectric nanogenerator for self-powered gesture recognition and language expression. Sci. Technol. Adv. Mater. *20*, 964–971.

Chung, H.U., Kim, B.H., Lee, J.Y., Lee, J., Xie, Z.Q., Ibler, E.M., Lee, K., Banks, A., Jeong, J.Y., Kim, J., et al. (2019). Binodal, wireless epidermal electronic systems with in-sensor analytics for neonatal intensive care. Science *363*, 947.

Cohen, D.J., Mitra, D., Peterson, K., and Maharbiz, M.M. (2012). A highly elastic, capacitive strain gauge based on percolating nanotube networks. Nano Lett. *12*, 1821–1825.

Cui, X., Cao, S., Yuan, Z., Xie, G., Ding, J., Sang, S., and Zhang, H. (2019). Electrode-free triboelectric nanogenerator for harvesting human biomechanical energy and as a versatile inartificial physiological monitor. Energy Technol. *7*, 1800931.

Cui, X., Zhang, C., Liu, W., Zhang, Y., Zhang, J., Li, X., Geng, L., and Wang, X. (2018). Pulse sensor based on single-electrode triboelectric nanogenerator. Sensors Actuat. A Phys. *280*, 326–331.

Ding, X., Cao, H., Zhang, X., Li, M., and Liu, Y. (2018). Large scale triboelectric nanogenerator and self-powered flexible sensor for human sleep monitoring. Sensors (Basel) *18*, 1713.

Dong, B., Yang, Y., Shi, Q., Xu, S., Sun, Z., Zhu, S., Zhang, Z., Kwong, D.L., Zhou, G., Ang, K.W., et al. (2020a). Wearable triboelectric-human-machine interface (THMI) using robust nanophotonic readout. ACS Nano *14*, 8915–8930.

Dong, K., Peng, X., An, J., Wang, A.C., Luo, J., Sun, B., Wang, J., and Wang, Z.L. (2020b). Shape adaptable and highly resilient 3D braided triboelectric nanogenerators as e-textiles for power and sensing. Nat. Commun. *11*, 2868.

Dong, K., Wu, Z., Deng, J., Wang, A.C., Zou, H., Chen, C., Hu, D., Gu, B., Sun, B., and Wang, Z.L. (2018). A stretchable yarn embedded triboelectric nanogenerator as electronic skin for biomechanical energy harvesting and multifunctional pressure sensing. Adv. Mater. *30*, e1804944.

Fan, F.R., Tian, Z.Q., and Wang, Z.L. (2012). Flexible triboelectric generator! Nano Energy *1*, 328–334.

Fan, W.J., He, Q., Meng, K.Y., Tan, X.L., Zhou, Z.H., Zhang, G.Q., Yang, J., and Wang, Z.L. (2020). Machine-knitted washable sensor array textile for precise epidermal physiological signal monitoring. Sci. Adv. *6*, eaay2840.

Fan, X., Chen, J., Yang, J., Bai, P., Li, Z.L., and Wang, Z.L. (2015). Ultrathin, rollable, paper-based triboelectric nanogenerator for acoustic energy harvesting and self-powered sound recording. ACS Nano *9*, 4236–4243.

Gao, W., Emaminejad, S., Nyein, H.Y.Y., Challa, S., Chen, K.V., Peck, A., Fahad, H.M., Ota, H., Shiraki, H., Kiriya, D., et al. (2016). Fully integrated wearable sensor arrays for multiplexed in situ perspiration analysis. Nature *529*, 509.

Gogurla, N., Roy, B., Park, J.-Y., and Kim, S. (2019). Skin-contact actuated single-electrode protein triboelectric nanogenerator and strain sensor for biomechanical energy harvesting and motion sensing. Nano Energy *62*, 674–681.

Guo, H., Wan, J., Wu, H., Wang, H., Miao, L., Song, Y., Chen, H., Han, M., and Zhang, H. (2020). Self-powered multifunctional electronic skin for a smart anti-counterfeiting signature system. ACS Appl. Mater. Inter. *12*, 22357–22364.

Guo, H.Y., Leng, Q., He, X.M., Wang, M.J., Chen, J., Hu, C.G., and Xi, Y. (2015). A triboelectric generator based on checker-like interdigital electrodes with a sandwiched PET thin film for harvesting sliding energy in all directions. Adv. Energy Mater. *5*, 1400790.

Guo, H.Y., Pu, X.J., Chen, J., Meng, Y., Yeh, M.H., Liu, G.L., Tang, Q., Chen, B.D., Liu, D., Qi, S., et al. (2018). A highly sensitive, self-powered triboelectric auditory sensor for social robotics and hearing aids. Sci. Robot. *3*, eaat2516.

Guo, X.H., Pei, W.H., Wang, Y.J., Chen, Y.F., Zhang, H., Wu, X., Yang, X.W., Chen, H.D., Liu, Y.Y., and Liu, R.C. (2016). A human-machine interface based on single channel EOG and patchable sensor. Biomed. Signal Proces. *30*, 98–105.

Han, Y., Yi, F., Jiang, C., Dai, K., Xu, Y., Wang, X., and You, Z. (2019). Self-powered gait pattern-based identity recognition by a soft and stretchable triboelectric band. Nano Energy *56*, 516–523.

He, H., Zeng, H., Fu, Y., Han, W., Dai, Y., Xing, L., Zhang, Y., and Xue, X. (2018a). A self-powered electronic-skin for real-time perspiration analysis and application in motion state monitoring. J. Mater. Chem. C *6*, 9624–9630.

He, T., Sun, Z., Shi, Q., Zhu, M., Anaya, D.V., Xu, M., Chen, T., Yuce, M.R., Thean, A.V.-Y., and Lee, C. (2019). Self-powered glove-based intuitive interface for diversified control applications in real/cyber space. Nano Energy *58*, 641–651.

He, X., Zou, H., Geng, Z., Wang, X., Ding, W., Hu, F., Zi, Y., Xu, C., Zhang, S.L., Yu, H., et al. (2018b). A hierarchically nanostructured cellulose fiber-based triboelectric nanogenerator for self-powered healthcare products. Adv. Funct. Mater. *28*, 1805540.

Huang, J., Yang, X., Yu, J., Han, J., Jia, C., Ding, M., Sun, J., Cao, X., Sun, Q., and Wang, Z.L. (2020). A universal and arbitrary tactile interactive system based on self-powered optical communication. Nano Energy *69*, 104419.

Hui, X.N., and Kan, E.C. (2018). Monitoring vital signs over multiplexed radio by near-field coherent sensing. Nat. Electron. *1*, 74–78.

Jang, J., Lee, J., Jang, J.H., and Choi, H. (2016). A triboelectric-based artificial basilar membrane to mimic cochlear tonotopy. Adv. Healthc. Mater. *5*, 2481–2487.

Jao, Y.-T., Yang, P.-K., Chiu, C.-M., Lin, Y.-J., Chen, S.-W., Choi, D., and Lin, Z.-H. (2018). A textile-based triboelectric nanogenerator with humidity-resistant output characteristic and its applications in self-powered healthcare sensors. Nano Energy *50*, 513–520.

Jeon, S.-B., Park, S.-J., Kim, W.-G., Tcho, I.-W., Jin, I.-K., Han, J.-K., Kim, D., and Choi, Y.-K. (2018). Self-powered wearable keyboard with fabric based triboelectric nanogenerator. Nano Energy *53*, 596–603.

Kang, H., Zhao, C., Huang, J., Ho, D.H., Megra, Y.T., Suk, J.W., Sun, J., Wang, Z.L., Sun, Q., and Cho, J.H. (2019). Fingerprint-inspired conducting hierarchical wrinkles for energy-harvesting E-skin. Adv. Funct. Mater. *29*, 1903580.

Kim, D.H., Ghaffari, R., Lu, N.S., Wang, S.D., Lee, S.P., Keum, H., D'Angelo, R., Klinker, L., Su, Y.W., Lu, C.F., et al. (2012). Electronic sensor and actuator webs for large-area complex geometry cardiac mapping and therapy. Proc. Natl. Acad. Sci. U S A *109*, 19910–19915.

Kim, I., Roh, H., and Kim, D. (2019). Willow-like portable triboelectric respiration sensor based on polyethylenimine-assisted CO2 capture. Nano Energy *65*, 103990.

Lai, Y.-C., Deng, J., Zhang, S.L., Niu, S., Guo, H., and Wang, Z.L. (2017). Single-thread-based wearable and highly stretchable triboelectric nanogenerators and their applications in cloth-based self-powered human-interactive and biomedical sensing. Adv. Funct. Mater. *27*, 1604462.

Lai, Y.C., Deng, J., Niu, S., Peng, W., Wu, C., Liu, R., Wen, Z., and Wang, Z.L. (2016). Electric eel-skin-inspired mechanically durable and super-stretchable nanogenerator for deformable power source and fully autonomous conformable electronic-skin applications. Adv. Mater. *28*, 10024–10032.

Lai, Y.C., Wu, H.M., Lin, H.C., Chang, C.L., Chou, H.H., Hsiao, Y.C., and Wu, Y.C. (2019). Entirely, intrinsically, and autonomously self-healable, highly transparent, and superstretchable triboelectric nanogenerator for personal power sources and self-powered electronic skins. Adv. Funct. Mater. *29*, 1904626.

Lee, Y., Cha, S.H., Kim, Y.W., Choi, D., and Sun, J.Y. (2018). Transparent and attachable ionic communicators based on self-cleanable triboelectric nanogenerators. Nat. Commun. *9*, 1804.

Li, W., Torres, D., Diaz, R., Wang, Z.J., Wu, C.S., Wang, C., Wang, Z.L., and Sepulveda, N. (2017). Nanogenerator-based dual-functional and self-powered thin patch loudspeaker or microphone for flexible electronics. Nat. Commun. *8*, 15310.

Lin, L., Wang, S.H., Xie, Y.N., Jing, Q.S., Niu, S.M., Hu, Y.F., and Wang, Z.L. (2013). Segmentally structured disk triboelectric nanogenerator for harvesting rotational mechanical energy. Nano Lett. *13*, 2916–2923.

Lin, Z., Wu, Z., Zhang, B., Wang, Y.-C., Guo, H., Liu, G., Chen, C., Chen, Y., Yang, J., and Wang, Z.L. (2019). A triboelectric nanogenerator-based smart insole for multifunctional gait monitoring. Adv. Mater. Technol. *4*, 1800360.

Lin, Z., Yang, J., Li, X., Wu, Y., Wei, W., Liu, J., Chen, J., and Yang, J. (2018). Large-scale and washable smart textiles based on triboelectric nanogenerator arrays for self-powered sleeping monitoring. Adv. Funct. Mater. *28*, 1704112.

Lipomi, D.J., Vosgueritchian, M., Tee, B.C.K., Hellstrom, S.L., Lee, J.A., Fox, C.H., and Bao, Z.N. (2011). Skin-like pressure and strain sensors based on transparent elastic films of carbon nanotubes. Nat. Nanotechnol. *6*, 788–792.

Liu, L., Yang, X., Zhao, L., Xu, W., Wang, J., Yang, Q., and Tang, Q. (2020). Nanowrinkle-patterned flexible woven triboelectric nanogenerator toward self-powered wearable electronics. Nano Energy *73*, 104797.

Liu, L.M., Pan, J., Chen, P.N., Zhang, J., Yu, X.H., Ding, X., Wang, B.J., Sun, X.M., and Peng, H.S. (2016). A triboelectric textile templated by a three-dimensionally penetrated fabric. J. Mater. Chem. A *4*, 6077–6083.

Liu, R., Kuang, X., Deng, J., Wang, Y.C., Wang, A.C., Ding, W., Lai, Y.C., Chen, J., Wang, P., Lin, Z., et al. (2018). Shape memory polymers for body motion energy harvesting and self-powered mechanosensing. Adv. Mater. *30*, 1705195.

Liu, Z., Ma, Y., Ouyang, H., Shi, B., Li, N., Jiang, D., Xie, F., Qu, D., Zou, Y., Huang, Y., et al. (2019a). Transcatheter self-powered ultrasensitive endocardial pressure sensor. Adv. Funct. Mater. *29*, 1807560.

Liu, Z., Zhao, Z., Zeng, X., Fu, X., and Hu, Y. (2019b). Expandable microsphere-based triboelectric nanogenerators as ultrasensitive pressure sensors for respiratory and pulse monitoring. Nano Energy *59*, 295–301.

Lu, X., Zheng, L., Zhang, H., Wang, W., Wang, Z.L., and Sun, C. (2020). Stretchable, transparent triboelectric nanogenerator as a highly sensitive self-powered sensor for driver fatigue and distraction monitoring. Nano Energy *78*, 105359.

Ma, Y.J., Choi, J., Hourlier-Fargette, A., Xue, Y.G., Chung, H.U., Lee, J.Y., Wang, X.F., Xie, Z.Q., Kang, D., Wang, H.L., et al. (2018). Relation between blood pressure and pulse wave velocity for human arteries. Proc. Natl. Acad. Sci. U S A *115*, 11144–11149.

Ma, Z., Wang, W., and Yu, D. (2020). Flexible textile-based self-driven sensor used for human motion monitoring. Energy Technol. *8*, 2000164.

Massaroni, C., Venanzi, C., Silvatti, A.P., Lo Presti, D., Saccomandi, P., Formica, D., Giurazza, F., Caponero, M.A., and Schena, E. (2018). Smart textile for respiratory monitoring and thoraco-abdominal motion pattern evaluation. J. Biophotonics *11*, e201700263.

Meng, K.Y., Chen, J., Li, X.S., Wu, Y.F., Fan, W.J., Zhou, Z.H., He, Q., Wang, X., Fan, X., Zhang, Y.X., et al. (2019). Flexible weaving constructed self-powered pressure sensor enabling continuous diagnosis of cardiovascular disease and measurement of cuffless blood pressure. Adv. Funct. Mater. *29*, 1806388.

Meng, Y., Zhao, J., Yang, X., Zhao, C., Qin, S., Cho, J.H., Zhang, C., Sun, Q., and Wang, Z.L. (2018). Mechanosensation-Active matrix based on direct-contact tribotronic planar graphene transistor array. ACS Nano *12*, 9381–9389.

Meyer, C., and Hickson, L. (2012). What factors influence help-seeking for hearing impairment and hearing aid adoption in older adults? Int. J. Audiol. *51*, 66–74.

Ohkuma, T., Ninomiya, T., Tomiyama, H., Kario, K., Hoshide, S., Kita, Y., Inoguchi, T., Maeda, Y., Kohara, K., Tabara, Y., et al. (2017). Brachial-ankle pulse wave velocity and the risk prediction of cardiovascular disease an individual participant data meta-analysis. Hypertension *69*, 1045.

Osborn, L.E., Dragomir, A., Betthauser, J.L., Hunt, C.L., Nguyen, H.H., Kaliki, R.R., and Thakor, N.V. (2018). Prosthesis with neuromorphic multilayered e-dermis perceives touch and pain. Sci. Robot. *3*, eaat3818.

Ouyang, H., Tian, J., Sun, G., Zou, Y., Liu, Z., Li, H., Zhao, L., Shi, B., Fan, Y., Fan, Y., et al. (2017). Self-powered pulse sensor for antidiastole of cardiovascular disease. Adv. Mater. *29*, 1703456.

Pang, C., Lee, G.Y., Kim, T.I., Kim, S.M., Kim, H.N., Ahn, S.H., and Suh, K.Y. (2012). A flexible and highly sensitive strain-gauge sensor using reversible interlocking of nanofibres. Nat. Mater. *11*, 795–801.

Park, S., Fukuda, K., Wang, M., Lee, C., Yokota, T., Jin, H., Jinno, H., Kimura, H., Zalar, P., Matsuhisa, N., et al. (2018). Ultraflexible near-infrared organic photodetectors for conformal photoplethysmogram sensors. Adv. Mater. *30*, 1802359.

Persano, L., Dagdeviren, C., Su, Y.W., Zhang, Y.H., Girardo, S., Pisignano, D., Huang, Y.G., and Rogers, J.A. (2013). High performance piezoelectric devices based on aligned arrays of nanofibers of poly (vinylidenefluoride-co-trifluoroethylene). Nat. Commun. *4*, 1633.

Popelka, M.M., Cruickshanks, K.J., Wiley, T.L., Tweed, T.S., Klein, B.E.K., and Klein, R. (1998). Low prevalence of hearing aid use among older adults with hearing loss: the epidemiology of hearing loss study. J. Am. Geriatr. Soc. *46*, 1075–1078.

Pu, X.J., Guo, H.Y., Chen, J., Wang, X., Xi, Y., Hu, C.G., and Wang, Z.L. (2017). Eye motion triggered self-powered mechnosensational communication system using triboelectric nanogenerator. Sci. Adv. *3*, e1700694.

Pu, X.J., Guo, H.Y., Tang, Q., Chen, J., Feng, L., Liu, G.L., Wang, X., Xi, Y., Hu, C.G., and Wang, Z.L. (2018). Rotation sensing and gesture control of a robot joint via triboelectric quantization sensor. Nano Energy *54*, 453–460.

Pu, X.J., Tang, Q., Chen, W.S., Huang, Z.Y., Liu, G.L., Zeng, Q.X., Chen, J., Guo, H.Y., Xin, L.M., and Hu, C.G. (2020). Flexible triboelectric 3D touch pad with unit subdivision structure for effective XY positioning and pressure sensing. Nano Energy *76*, 105047.

Ren, Z., Nie, J., Shao, J., Lai, Q., Wang, L., Chen, J., Chen, X., and Wang, Z.L. (2018). Fully elastic and metal-free tactile sensors for detecting both normal and tangential forces based on triboelectric nanogenerators. Adv. Funct. Mater. *28*, 1802989.

Said, M.A., Eppinga, R.N., Lipsic, E., Verweij, N., and van der Harst, P. (2018). Relationship of arterial stiffness index and pulse pressure with cardiovascular disease and mortality. J. Am. Heart Assoc. *7*, e007621.

Sarkar, P.K., Kamilya, T., and Acharya, S. (2019). Introduction of triboelectric positive bioplastic for powering portable electronics and self-powered gait sensor. ACS Appl. Energy Mater. *2*, 5507–5514.

Shi, Q., Zhang, Z., Chen, T., and Lee, C. (2019a). Minimalist and multi-functional human machine interface (HMI) using a flexible wearable triboelectric patch. Nano Energy *62*, 355–366.

Shi, Q.F., He, T.Y.Y., and Lee, C. (2019b). More than energy harvesting - combining triboelectric nanogenerator and flexible electronics technology for enabling novel micro-/nano-systems. Nano Energy *57*, 851–871.

Si, Y.J., Li, F.L., Duan, K.Y., Tao, Q., Li, C.B., Cao, Z.H., Zhang, Y.S., Biswal, B., Li, P.Y., Yao, D.Z., et al. (2020). Predicting individual decision-making responses based on single-trial EEG. Neuroimage *206*, 116333.

Sun, J.-G., Yang, T.-N., Wang, C.-Y., and Chen, L.-J. (2018). A flexible transparent one-structure tribo-piezo-pyroelectric hybrid energy generator based on bio-inspired silver nanowires network for biomechanical energy harvesting and physiological monitoring. Nano Energy *48*, 383–390.

Usakli, A.B., and Gurkan, S. (2010). Design of a novel efficient human-computer interface: an electrooculagram based virtual keyboard. IEEE Trans. Instrum. Meas. *59*, 2099–2108.

Vera Anaya, D., He, T., Lee, C., and Yuce, M.R. (2020). Self-powered eye motion sensor based on triboelectric interaction and near-field electrostatic induction for wearable assistive technologies. Nano Energy *72*, 104675.

Wang, P., Liu, R., Ding, W., Zhang, P., Pan, L., Dai, G., Zou, H., Dong, K., Xu, C., and Wang, Z.L. (2018a). Complementary electromagnetic-triboelectric active sensor for detecting multiple mechanical triggering. Adv. Funct. Mater. *28*, 1705808.

Wang, S., He, M., Weng, B., Gan, L., Zhao, Y., Li, N., and Xie, Y. (2018b). Stretchable and wearable triboelectric nanogenerator based on kinesio tape for self-powered human motion sensing. Nanomaterials (Basel) *8*, 657.

Wang, S., Jiang, Y., Tai, H., Liu, B., Duan, Z., Yuan, Z., Pan, H., Xie, G., Du, X., and Su, Y. (2019a). An integrated flexible self-powered wearable respiration sensor. Nano Energy *63*, 103829.

Wang, S., Tai, H., Liu, B., Duan, Z., Yuan, Z., Pan, H., Su, Y., Xie, G., Du, X., and Jiang, Y. (2019b). A facile respiration-driven triboelectric nanogenerator for multifunctional respiratory monitoring. Nano Energy *58*, 312–321.

Wang, S.H., Xu, J., Wang, W.C., Wang, G.J.N., Rastak, R., Molina-Lopez, F., Chung, J.W., Niu, S.M., Feig, V.R., Lopez, J., et al. (2018c). Skin electronics from scalable fabrication of an intrinsically stretchable transistor array. Nature *555*, 83.

Wang, X., Zhang, H., Dong, L., Han, X., Du, W., Zhai, J., Pan, C., and Wang, Z.L. (2016). Self-powered high-resolution and pressure-sensitive triboelectric sensor matrix for real-time tactile mapping. Adv. Mater. *28*, 2896–2903.

Wang, X.W., Gu, Y., Xiong, Z.P., Cui, Z., and Zhang, T. (2014). Silk-molded flexible, ultrasensitive, and highly stable electronic skin for monitoring human physiological signals. Adv. Mater. *26*, 1336–1342.

Wang, Z., An, J., Nie, J., Luo, J., Shao, J., Jiang, T., Chen, B., Tang, W., and Wang, Z.L. (2020). A self-powered angle sensor at nanoradian-resolution for robotic arms and personalized medicare. Adv. Mater. *32*, e2001466.

Wang, Z.L. (2013). Triboelectric nanogenerators as new energy technology for self-powered systems and as active mechanical and chemical sensors. ACS Nano *7*, 9533–9557.

Wang, Z.L. (2017). On Maxwell's displacement current for energy and sensors: the origin of nanogenerators. Mater. Today *20*, 74–82.

Wang, Z.L. (2020a). On the first principle theory of nanogenerators from Maxwell's equations. Nano Energy *68*, 104272.

Wang, Z.L. (2020b). Triboelectric nanogenerator (TENG)-Sparking an energy and sensor revolution. Adv. Energy Mater. *10*, 2000137.

Wang, Z.L., and Song, J.H. (2006). Piezoelectric nanogenerators based on zinc oxide nanowire arrays. Science *312*, 242–246.

Wang, Z.L., and Wang, A.C. (2019). On the origin of contact-electrification. Mater. Today *30*, 34–51.

Wang, Z.L., Zhu, G., Yang, Y., Wang, S.H., and Pan, C.F. (2012). Progress in nanogenerators for portable electronics. Mater. Today *15*, 532–543.

Wu, C., Kim, T.W., Park, J.H., Koo, B., Sung, S., Shao, J., Zhang, C., and Wang, Z.L. (2020). Self-powered tactile sensor with learning and memory. ACS Nano *14*, 1390–1398.

Wu, C.S., Ding, W.B., Liu, R.Y., Wang, J.Y., Wang, A.C., Wang, J., Li, S.M., Zi, Y.L., and Wang, Z.L. (2018a). Keystroke dynamics enabled authentication and identification using triboelectric nanogenerator array. Mater. Today *21*, 216–222.

Wu, H., Shi, Q., Wang, F., Thean, A.V.-Y., and Lee, C. (2018b). Self-powered cursor using a triboelectric mechanism. Small Methods *2*, 1800078.

Wu, H., Su, Z., Shi, M., Miao, L., Song, Y., Chen, H., Han, M., and Zhang, H. (2017). Self-powered noncontact electronic skin for motion sensing. Adv. Funct. Mater. *28*, 1704641.

Wu, W.Z., Wen, X.N., and Wang, Z.L. (2013). Taxel-addressable matrix of vertical-nanowire piezotronic transistors for active and adaptive tactile imaging. Science *340*, 952–957.

Xu, W., Huang, L.-B., Wong, M.-C., Chen, L., Bai, G., and Hao, J. (2017). Environmentally friendly hydrogel-based triboelectric nanogenerators for

versatile energy harvesting and self-powered sensors. Adv. Energy Mater. *7*, 1601529.

Xu, W.H., Zheng, H.X., Liu, Y., Zhou, X.F., Zhang, C., Song, Y.X., Deng, X., Leung, M., Yang, Z.B., Xu, R.X., et al. (2020). A droplet-based electricity generator with high instantaneous power density. Nature *578*, 392.

Xue, F., Chen, L., Wang, L., Pang, Y., Chen, J., Zhang, C., and Wang, Z.L. (2016). MoS2Tribotronic transistor for smart tactile switch. Adv. Funct. Mater. *26*, 2104–2109.

Yan, C., Deng, W., Jin, L., Yang, T., Wang, Z., Chu, X., Su, H., Chen, J., and Yang, W. (2018). Epidermis-inspired ultrathin 3D cellular sensor array for self-powered biomedical monitoring. ACS Appl. Mater. Inter. *10*, 41070–41075.

Yang, G.Z., Bellingham, J., Dupont, P.E., Fischer, P., Floridi, L., Full, R., Jacobstein, N., Kumar, V., McNutt, M., Merrifield, R., et al. (2018). The grand challenges of Science Robotics. Sci. Robot. *3*, eaar7650.

Yang, J., Chen, J., Su, Y., Jing, Q., Li, Z., Yi, F., Wen, X., Wang, Z., and Wang, Z.L. (2015a). Eardrum-inspired active sensors for self-powered cardiovascular system characterization and throat-attached anti-interference voice recognition. Adv. Mater. *27*, 1316–1326.

Yang, P.K., Lin, L., Yi, F., Li, X., Pradel, K.C., Zi, Y., Wu, C.I., He, J.H., Zhang, Y., and Wang, Z.L. (2015b). A flexible, stretchable and shape-adaptive approach for versatile energy conversion and self-powered biomedical monitoring. Adv. Mater. *27*, 3817–3824.

Yang, Y., Zhang, H.L., Lin, Z.H., Zhou, Y.S., Jing, Q.S., Su, Y.J., Yang, J., Chen, J., Hu, C.G., and Wang, Z.L. (2013). Human skin based triboelectric nanogenerators for harvesting biomechanical energy and as self-powered active tactile sensor system. ACS Nano *7*, 9213–9222.

Yi, F., Lin, L., Niu, S., Yang, P.K., Wang, Z., Chen, J., Zhou, Y., Zi, Y., Wang, J., Liao, Q., et al. (2015). Stretchable-rubber-based triboelectric nanogenerator and its application as self-powered body motion sensors. Adv. Funct. Mater. *25*, 3688–3696.

Yi, F., Wang, X.F., Niu, S.M., Li, S.M., Yin, Y.J., Dai, K.R., Zhang, G.J., Lin, L., Wen, Z., Guo, H.Y., et al. (2016). A highly shape-adaptive, stretchable design based on conductive liquid for energy harvesting and self-powered biomechanical monitoring. Sci. Adv. *2*, e1501624.

Yu, H., He, X., Ding, W.B., Hu, Y.S., Yang, D.C., Lu, S., Wu, C.S., Zou, H.Y., Liu, R.Y., Lu, C.H., et al. (2017). A self-powered dynamic displacement monitoring system based on triboelectric accelerometer. Adv. Energy Mater. *7*, 1700565.

Yu, J., Hou, X., Cui, M., Shi, S., He, J., Sun, Y., Wang, C., and Chou, X. (2019). Flexible PDMS-based triboelectric nanogenerator for instantaneous force sensing and human joint movement monitoring. Sci. China Mater. *62*, 1423–1432.

Yuan, Z., Zhou, T., Yin, Y., Cao, R., Li, C., and Wang, Z.L. (2017). Transparent and flexible triboelectric sensing array for touch security applications. ACS Nano *11*, 8364–8369.

Zhang, C., Tang, W., Pang, Y.K., Han, C.B., and Wang, Z.L. (2015). Active micro-actuators for optical modulation based on a planar sliding triboelectric nanogenerator. Adv. Mater. *27*, 719–726.

Zhang, H., Zhang, J., Hu, Z., Quan, L., Shi, L., Chen, J., Xuan, W., Zhang, Z., Dong, S., and Luo, J. (2019a). Waist-wearable wireless respiration sensor based on triboelectric effect. Nano Energy *59*, 75–83.

Zhang, R., Hummelgård, M., Örtegren, J., Yang, Y., Andersson, H., Balliu, E., Blomquist, N., Engholm, M., Olsen, M., Wang, Z.L., et al. (2019b). Sensing body motions based on charges generated on the body. Nano Energy *63*, 103842.

Zhang, S.L., Lai, Y.C., He, X., Liu, R.Y., Zi, Y.L., and Wang, Z.L. (2017). Auxetic foam-based contact-mode triboelectric nanogenerator with highly sensitive self-powered strain sensing capabilities to monitor human body movement. Adv. Funct. Mater. *27*, 1606695.

Zhang, X.S., Han, M.D., Wang, R.X., Zhu, F.Y., Li, Z.H., Wang, W., and Zhang, H.X. (2013). Frequency-multiplication high-output triboelectric nanogenerator for sustainably powering biomedical microsystems. Nano Lett. *13*, 1168–1172.

Zhao, G., Zhang, Y., Shi, N., Liu, Z., Zhang, X., Wu, M., Pan, C., Liu, H., Li, L., and Wang, Z.L. (2019). Transparent and stretchable triboelectric nanogenerator for self-powered tactile sensing. Nano Energy *59*, 302–310.

Zhao, X., Zhang, Z., Liao, Q.L., Xun, X.C., Gao, F.F., Xu, L.X., Kang, Z., and Zhang, Y. (2020). Self-powered user-interactive electronic skin for programmable touch operation platform. Sci. Adv. *6*, eaba4294.

Zhao, Z., Yan, C., Liu, Z., Fu, X., Peng, L.M., Hu, Y., and Zheng, Z. (2016). Machine-washable textile triboelectric nanogenerators for effective human respiratory monitoring through loom weaving of metallic yarns. Adv. Mater. *28*, 10267–10274.

Zheng, Q., Tang, Q.Z., Wang, Z.L., and Li, Z. (2020). Self-powered cardiovascular electronic devices and systems. Nat. Rev. Cardiol. *18*, 7–21.

Zhong, Q.Z., Zhong, J.W., Hu, B., Hu, Q.Y., Zhou, J., and Wang, Z.L. (2013). A paper-based nanogenerator as a power source and active sensor. Energ Environ. Sci. *6*, 1779–1784.

Zhou, L.L., Liu, D., Wang, J., and Wang, Z.L. (2020). Triboelectric nanogenerators: Fundamental physics and potential applications. Friction *8*, 481–506.

Zhou, Y.S., Zhu, G., Niu, S.M., Liu, Y., Bai, P.S., Jing, Q., and Wang, Z.L. (2014). Nanometer resolution self-powered static and dynamic motion sensor based on micro-grated triboelectrification. Adv. Mater. *26*, 1719–1724.

Zhu, M.L., Sun, Z.D., Zhang, Z.X., Shi, Q.F., He, T.Y.Y., Liu, H.C., Chen, T., and Lee, C.K. (2020). Haptic-feedback smart glove as a creative human-machine interface (HMI) for virtual/augmented reality applications. Sci. Adv. *6*, eaaz8693.

Zou, Y., Tan, P.C., Shi, B.J., Ouyang, H., Jiang, D.J., Liu, Z., Li, H., Yu, M., Wang, C., Qu, X.C., et al. (2019). A bionic stretchable nanogenerator for underwater sensing and energy harvesting. Nat. Commun. *10*, 2695.